Binding of 5-Phospho-D-Arabinonohydroxamate and 5-Phospho-D-Arabinonate Inhibitors to Zinc Phosphomannose Isomerase from *Candida albicans* Studied by Polarizable Molecular Mechanics and Quantum Mechanics

CELINE ROUX,[1] NOHAD GRESH,[2] LALITH E. PERERA,[3] JEAN-PHILIP PIQUEMAL,[3,4] LAURENT SALMON[1]

[1]*Laboratoire de Chimie Bioorganique et Bioinorganique, CNRS-UMR 8182, Institut de Chimie Moléculaire et des Matériaux d'Orsay, Bâtiment 420, Université Paris-Sud XI, 15 rue Georges Clémenceau, 91405 Orsay, France*

[2]*Laboratoire de Pharmacochimie Moléculaire et Cellulaire, INSERM U648, IFR Biomédicale, Université René Descartes, 45 rue des Saint-Pères, 75006 Paris, France*

[3]*Laboratory of Structural Biology, National Institute of Environmental Health Sciences, 111 Alexander Drive, Research Triangle Park, North Carolina 27700*

[4]*Laboratoire de Chimie Theorique, UMR 7616 CNRS, Universite Pierre et Marie Curie, CC 137, 4, Place Jussieu, 75252 Paris Cedex 05*

Received 15 September 2005; Accepted 8 June 2006
DOI 10.1002/jcc.20586
Published online 25 January 2007 in Wiley InterScience (www.interscience.wiley.com).

Abstract: Type I phosphomannose isomerase (PMI) is a Zn-dependent metalloenzyme involved in the isomerization of D-fructose 6-phosphate to D-mannose 6-phosphate. One of our laboratories has recently designed and synthesized 5-phospho-D-arabinonohydroxamate (5PAH), an inhibitor endowed with a nanomolar affinity for PMI (Roux et al., Biochemistry 2004, 43, 2926). By contrast, the 5-phospho-D-arabinonate (5PAA), in which the hydroxamate moiety is replaced by a carboxylate one, is devoid of inhibitory potency. Subsequent biochemical studies showed that in its PMI complex, 5PAH binds Zn(II) through its hydroxamate moiety rather than through its phosphate. These results have stimulated the present theoretical investigation in which we resort to the SIBFA polarizable molecular mechanics procedure to unravel the structural and energetical aspects of 5PAH and 5PAA binding to a 164-residue model of PMI. Consistent with the experimental results, our theoretical studies indicate that the complexation of PMI by 5PAH is much more favorable than by 5PAA, and that in the 5PAH complex, Zn(II) ligation by hydroxamate is much more favorable than by phosphate. Validations by parallel quantum-chemical computations on model of the recognition site extracted from the PMI-inhibitor complexes, and totaling up to 140 atoms, showed the values of the SIBFA intermolecular interaction energies in such models to be able to reproduce the quantum-chemistry ones with relative errors $< 3\%$. On the basis of the PMI–5PAH SIBFA energy-minimized structure, we report the first hypothesis of a detailed view of the active site of the zinc PMI complexed to the high-energy intermediate analogue inhibitor, which allows us to identify active site residues likely involved in the proton transfer between the two adjacent carbons of the substrates.

 J Comput Chem 28: 938–957, 2007

Key words: phosphomannose isomerase; Zn(II) cation; polarizable molecular mechanics; *ab initio* computations; enzyme inhibitors; hydroxamates

Introduction

Phosphomannose isomerase (PMI, EC 5.3.1.8), originally discovered from Baker's yeast by Slein[1] and characterized by Gracy and Noltmann[2] is a metal-dependent aldose–ketose isomerase that catalyzes the reversible isomerization of D-mannose 6-phosphate (M6P) and D-fructose-6-phosphate (F6P; Fig. 1). In all

Correspondence to: N. Gresh; e-mail: nohad.gresh@univ-paris5.fr or L. Salmon; e-mail: lasalmon@icmo.u-psud.fr

Contract/grant sponsors: Ligue Nationale contre le Cancer (Comité de Paris), NIH, NIEHS

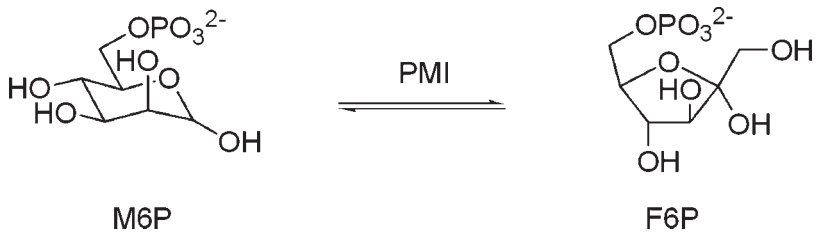

Figure 1. Molecular structures of D-mannose 6-phosphate and of D-fructose-6-phosphate.

organisms investigated so far, PMI is reported to play a crucial role in both D-mannose metabolism and the supply of the activated mannose donor guanosine diphosphate D-mannose (GDP-D-mannose), which is a required reactant for the biosynthesis of many mannosylated structures,[3] including glycoproteins, glycolipids, and in the case of microorganisms such as fungi, cell wall components. Following PMI-catalyzed isomerization of F6P to M6P and subsequent conversion of M6P to D-mannose-1-phosphate by phosphomannomutase, incorporation of GTP by GDP-D-mannose pyrophosphorylase (GMP) yields GDP-D-mannose. Provided, there are significant differences in amino acid sequence between PMIs from pathogens and humans, these enzymes are considered to be potential therapeutic targets because of their role in the virulence or survival of cells from several microorganisms, including *Saccharomyces cerevisiae*,[4] *Candida albicans*,[5] *Mycobacterium smegmatis*,[6] the protozoan parasite *Leishmania mexicana*,[7] and *Pseudomonas aeruginosa*.[8] Indeed, fungal and bacterial infections can lead to serious illness and death in immunosuppressed individuals. Cutaneous, mucocutaneous, and visceral leishmaniasis is a worldwide disease, with a clear increasing number of cases. Mucoid strains of *P. aeruginosa* cause recurrent and life-threatening lung infections in cystic fibrosis patients, where PMI has been reported to be essential in the production of alginate, an exopolysaccharide which protects bacteria from antibiotics and the host's immune system.

From sequence alignments and physicochemical and kinetic characterizations, it has been proposed that the PMIs comprise three families of proteins: type I, type II, and type III PMIs.[9] Members of all three families share little or no sequence identity, except for a very small conserved amino acid sequence motif, which makes up part of the active site.[10] Type I PMIs, which include proteins from *Aspergillus nidulans*,[11] *Candida albicans*,[12–16] *Cryptococcus neoformans*,[17] *Escherichia coli*,[18] *Homo sapiens*,[15] *Saccharomyces cerevisiae*,[9,15,19–21] *Salmonella typhimurium*,[22] and *Streptococcus mutans*,[10] are homologous monofunctional enzymes catalyzing the single reversible isomerization reaction of M6P to F6P. The type I PMI isolated from *Saccharomyces cerevisiae* in 1968[2] has been shown to be a zinc-dependent metalloenzyme, with one metal atom per molecule of the 45 kD monomer.[23] Type II PMIs are bifunctional enzymes possessing both PMI and GMP activities in separate catalytic domains.[10] The enzymes reported so far are found only in some bacteria, including *Acetobacter xylinum*,[24] *Acinetobacter calcoaceticus*,[10] *Helicobacter pylori*,[25] *Pseudomonas aeruginosa*,[8] *Rhodospirillium rubrum*,[26] *Salmonella typhimurium*,[22,27] and *Xanthomonas campestris*.[28] PMI activity in type II enzymes uses Zn^{2+} as metal cofactor, but also can use other divalent cations, Co^{2+}, Mg^{2+}, Mn^{2+}, Ca^{2+}, or Ni^{2+}, depending on the enzyme source. So far only one type III PMI has been reported, from *Rhizobium meliloti*.[29] A fourth type of PMI might be proposed within the phosphoglucose isomerase (PGI, E.C. 5.3.1.9) superfamily, where several aerobic crenarchaeons, including *Aeropyrum pernix*,[30] *Pyrobaculum aerophilum*,[31] and *Thermoplasma acidophilum*,[30] have been shown to display an atypical dual-specificity PGI/PMI. PGI is the aldose–ketose isomerase that catalyzes the reversible isomerization of glucose 6-phosphate (G6P) to F6P.[32] Except for *Pyrococcus furiosis*,[33,34] PGIs do not require a metal cofactor for activity. High-resolution X-ray crystal structures have shown a high degree of conservation between the active site residues of the archaeon PGI/PMI from *Aeropyrum pernix* and those of bacterial and eukaryotic PGIs, which cannot isomerize M6P to F6P except at an extremely low rate.[35] PMI activity, which proceeds at an equal rate as PGI activity, appears to arise from a subtle difference in the architecture of the PMI/PGI enzyme, compared to conventional PGIs.[36,37]

The catalytic mechanism of PGIs has been extensively studied and is now quite well defined.[38–43] However, in the case of conventional PMIs (types I, II, III), it is yet to be established. Through temperature dependence experiments of the isotope effect observed for the hydrogen-transfer ratio, the mechanism is known to proceed through a proton transfer between the two carbon atoms C1 and C2 and to involve a 1,2-*cis*-enediolate high-energy intermediate,[44] analogous to the PGI catalyzed isomerization.[32] However, PMI stereospecifically abstracts the pro-*S* proton of F6P, whereas it is the pro-*R* for PGI. Only one high-resolution X-ray crystal structure of a PMI (type I *Candida albicans*) has been reported to date, with no substrate or inhibitor complexed at the active site.[13] A pocket on the surface that is very likely to be the active site and a zinc metal cofactor binding site has been identified; however, the role of the individual active site amino acids is still not known.[13] The mechanism of the PMI-catalyzed reversible isomerization of M6P to F6P is likely to be distinct from that catalyzed by the archaeon PGI/PMI, because all known PMIs are metalloenzymes and typically contain a Zn^{2+} that is required for catalysis.[37] Cleasby et al. suggested that the metal cofactor may play an active part in catalyzing the reaction, since the enzyme can be protected by substrate from inactivation by metal chelators, rather than merely maintaining the structural integrity of the enzyme.[13] In addition, PMIs are known to have no anomerase or epimerase activity, in contrast to PGIs,[35] which could be explained by the coordination of the C1 and C2 O atoms of M6P and F6P by the zinc atom, preventing rotations of the substrate's bonds. Indeed, we recently

Figure 2. Molecular structures of 5-phospho-D-arabinonohydroxamate (5PAH) and 5-phospho-D-arabinonate (5PAA).

reported 5-phospho-D-arabinonohydroxamate (5PAH, Fig. 2) as the most potent inhibitor of both yeast type I and *Pseudomonas aeruginosa* type II PMIs.[45] We therefore proposed an enzyme-inhibitor complex in which the zinc cofactor would be coordinated to the hydroxamate function, which is a mimic of the enediolate moiety of the reaction intermediate. In contrast, 5-phospho-D-arabinonate (5PAA, Fig. 2) was reported not to inhibit either PMI. Through comparison to the case of PGI where 5PAH and 5PAA are both strong inhibitors, we reported these results as consistent with a catalytic role for the metal cofactor, in accord with the initial mechanistic hypothesis reported by Gracy and Noltmann.[46] Nevertheless, no conclusive experimental evidence supports this hypothesis, and a detailed mechanism for the PMI catalyzed isomerization of M6P to F6P remains to be proposed. No high-resolution X-ray structure of a metal-dependent PMI complexed to the postulated high-energy intermediate analogue inhibitor 5PAH has been reported yet. Hence, there is no direct evidence of the binding mode of the inhibitor to the zinc active site of the enzyme. As mentioned above, the nature and role of the amino acids directly involved in the reaction mechanism are not known, and particularly the catalytic base involved in the proton transfer between the two carbons of the substrates M6P and F6P. Finally, the reason why 5PAA, a strong PGI inhibitor, does not inhibit PMI is still unclear.[45]

In order to address these issues, we report in this paper a molecular modeling study of the enzyme complexed with 5PAH and 5PAA. For each inhibitor, two competing binding modes of the bifunctional inhibitors to the active site zinc were considered: (i) binding of the phosphate part, (ii) binding of the hydroxamate (5PAH) or carboxylate (5PAA) part. The three-dimensional structure of type I PMI from *Candida albicans* reported by Cleasby et al.[13] (Fig. 3), the only metal-dependent PMI structure available (PDB ID code: 1PMI), was used as a starting point to generate a theoretical model of the enzyme, and thereafter the four complexes of the model with 5PAH and 5PAA. Kinetic and physicochemical studies on type I PMIs have shown that they have very similar characteristics.[15] The protein shows a high level of sequence identity (>40%) with type I PMI genes cloned from other species,[9] particularly in the region of the active site, so that conclusions that may be drawn from *C. albicans* PMI can most likely be applied for other type I PMIs, including yeast and human PMIs. Consequently, although 5PAH will probably not by itself be a clinically useful drug, it may serve as a starting point for drug design by enabling the identification of the most important protein-inhibitor interactions. We used the polarizable molecular mechanics procedure SIBFA (Sum of Interactions Between Fragments *ab initio* computed) to study PMI-inhibitor interactions. Although *ab initio* quantum chemistry (QC) is the most accurate procedure for computation of intermolecular interactions, with currently available softwares it cannot be applied to systematically investigate very large complexes (more than 200 atoms). The SIBFA procedure has been formulated and calibrated on the basis of *ab initio* QC calculations.[48] It was successfully applied to study various polyligated Zn(II) complexes, including complexes of inhibitors with thermolysin,[49,50] and β-lactamase[51,52] metalloenzymes, that of an ATP analogue with a bacterial kinase,[53] the complexes of Zn(II) and Zn(II)-pentahydrates with nucleic acid bases and

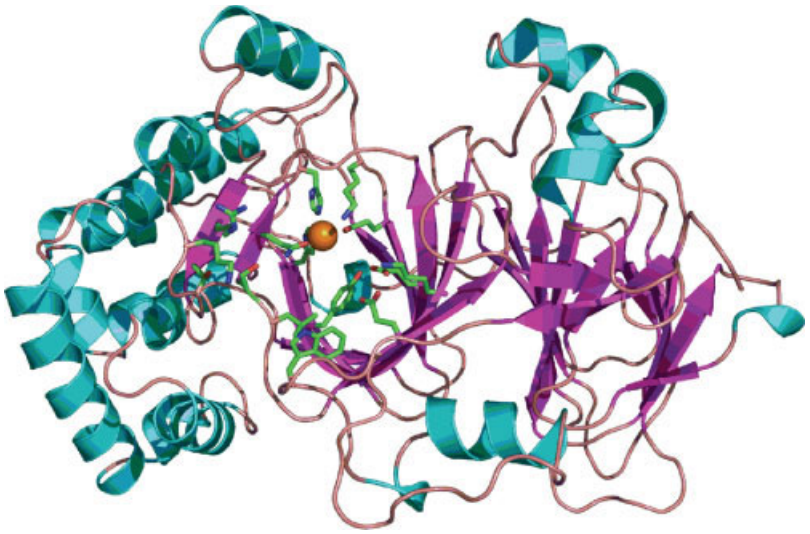

Figure 3. Representation of the three-dimensional structure of *Candida albicans* PMI from high-resolution X-ray crystallography (from Cleasby et al.[13]). Image was made using the program PyMOL.[47] [Color figure can be viewed in the online issue, which is available at www.interscience.wiley.com.]

guanosine mononucleotide,[54,55] and towards *de novo* predictions of the conformation of 18-residue long-Zn fingers.[56] It was recently refined by the inclusion of a "penetration" component to the electrostatic multipolar contribution.[57,58] Validation studies by parallel QC computations on model complexes showed the QC intermolecular ΔE's to be reproduced with relative errors $< 3\%$.[58] With more than 4000 atoms, PMI represents one of the largest biomolecules so far studied by the SIBFA procedure. The energy balances include the inter- and intramolecular interaction energies and the contribution from solvation computed using a Continuum reaction field procedure, namely the Langlet–Claverie (LC) procedure.[59] Consistent with SIBFA, the LC procedure computes the electrostatic and polarization contributions of ΔG_{solv} with the same set of distributed multipoles as SIBFA, which should ensure for the mutual consistency in the two approaches. On the basis of the energy balances, we will attempt to account for the preferential binding of 5PAH to the Zn(II)-binding site through its hydroxamate rather than through its phosphate moiety, and for the stronger PMI-binding affinity of 5PAH than 5PAA.

Procedure

SIBFA Computations

The intermolecular interaction energy was computed as a sum of five components: electrostatic multipolar energy (E_{MTP}), short-range repulsion (E_{rep}), polarization (E_{pol}), charge-transfer (E_{ct}), and dispersion (E_{disp}). The expression of each contribution was detailed in our previous papers.[48,57,58] Following the recent refinements published,[57,58] E_{MTP} is augmented with a "penetration" component E_{pen}, an attractive, overlap-dependent term arising in coulomb interactions when electron clouds overlap. The expression for E_{pen} in SIBFA, and the refinements of E_{rep} were previously given.[57,58] The values of the parameters have been previously detailed.[58]

Calculation of Solvation Energies ΔG_{solv}

ΔG_{solv} was computed using the LC procedure[59] interfaced in SIBFA.[60] It is formulated as a sum of electrostatic, polarization, repulsion, dispersion and cavitation contributions. Their expressions were given in the original paper.[59] Briefly, the electrostatic term is the energy due to the interaction between the electrostatic potential V created by the distributed multipoles of the solute and a fictitious charge density distributed on the cavity surface S. The charge density at a given point of S is a function of the solvent dielectric constant and of the scalar product between the electric field created between the solute multipoles and the unitary vector normal to the surface at that point. The polarization energy of each solute polarizable center is a function of its polarizability and of the square of the solvent reaction field created on that center by the charge density. In keeping with Langlet et al.,[60] we use scalar polarizabilities distributed on heteroatoms and bond barycenters rather than the Garmer–Stevens polarizabilities[61] used for the SIBFA inter- or intramolecular interaction energies. Following the derivation by Huron and Claverie,[62] the repulsion and dispersion terms are computed as sums of repulsion and dispersion energy volume integrals. The sums run on the solute atoms i, on the one hand, and on the solvent types of atoms j, on the other hand. The cavitation energy is calculated as a sum of contributions from intersecting spheres, centered on the solute atoms. Following a formulation due to Pierotti,[63] it is a function (up to quadratic) of a quantity d, which is the sum of the diameters of the considered atom-centered sphere and of the solvent sphere.

Calibration

We have been prompted by the remarks by one reviewer to search for an improved calibration of ΔG_{solv} that could be based on comparisons with corresponding quantum-chemical continuum methodologies, such as the quantum-chemical implementation of the Poisson–Boltzmann (PB) procedure by Tannor et al.,[64] and the polarizable continuum model (PCM) by Tomasi and Persico.[65] In the latter, ΔG_{solv} is formulated as a sum of terms related to the LC ones. Additional refinements of the LC procedure that iteratively include the contributions to the solute electrostatic potential of the dipoles induced on it by the reaction field of the solvent are underway. Thus for the present purposes, we did not seek a term-to-term agreement with the PCM components in the present stage, and were more concerned with an agreement in terms of the total ΔG_{solv}(LC) with both corresponding PB and PCM approaches for a diversity of model ionic, polar, and apolar solutes (discussed below). In the previous calibration, the van der Waals surface of the cavity was multiplied by a factor λ of 1.2. We have found that a significant improvement in the match of ΔG_{solv}(LC) with its QC counterpart could be obtained by small modulations of this value as a function of the chemical nature of the solute. The following values for λ were adopted: polar: 1.1; mono- and dianionic: 1.1; cationic: 1.1; divalent (Zn(II)): 1.2; conjugated: 1.24; aliphatic: 1.20. The three other parameters are the exponent of the repulsion term (11.40, left unchanged) and the multiplicative factors of the repulsion and dispersion terms. These were changed from 28,780.0 (E_{rep}) and 0.29 (E_{disp}) to 3299.0 and 0.161, respectively.

Construction of the Protein and of the Inhibitors

The protein was assembled with the standard library of its constitutive backbone and side-chain fragments, encompassing the internal coordinates and the distributed multipoles and polarizabilities. Based on a 15 Å proximity criterion to Zn(II), a 164-residue model was assembled. It was built out of the six oligopeptide sequences: Asn15-Gly19, Tyr46-His54, Phe97-Lys153, Val205-Asn211, Gly258-Met333, and Asp352-Leu361. Since we are interested in relative energy differences, and the excluded PMI residues are far from the recognition site, it can be expected that resorting to a truncated rather than integral PMI model should affect in similar fashion the differing competing 5PAH and 5PAA complexes. This is supported by the conclusions obtained in our first study of inhibitor binding to metallo-β-lactamase, a binuclear Zn-dependent bacterial metalloenzyme.[51] In this study, the energy balances of nine competing complexes of D- and L-captopril to a 104-residue model of this

enzyme were compared. The ordering of their relative affinities was unchanged upon extending the model to 188 residues, except for an inversion between two D-captopril complexes, whose relative energy differences were <2 kcal/mol. The 5PAH was built out of formohydroxamate ($HCONHO^-$), methane, water, and hydrogenophosphonate (HPO_3^{2-}) fragments. The 5PAA was built using the same fragments, with formate ($HCOO^-$) replacing formohydroxamate. Standard bond lengths and valence angles were used.

Treatment of Flexible Molecules

We have resorted to a procedure that was developed and tested in recent studies of Zn(II) finger oligopeptides,[56] pentahydrated Zn(II) and Mg(II) complexes of 5′-guanosine monophosphate,[55] organometallic complexes of Cu(II),[66] conformational studies of eleven model alanine and glycine tetrapeptides,[67] and the complexes of metallo-β-lactamase with captopril and thiomandelate.[52] Earlier tests published on Zn(II)-binding to neutral and zwitterionic glycine,[68] α- and β-mercaptoxamides,[69] and pyrophosphate[53] had shown such a procedure to provide interaction energy values having relative errors wih respect to their QC counterparts of $< 3\%$, which are similar to those from the approach treating the integral Zn-binding ligand with its conformation-specific multipoles and polarizabilities. Thus to compute E_{MTP}, the multipoles were redistributed at the junctions between fragments following the reported procedure.[70] To compute E_{pol}, the multipoles of the interfragment junctional bonds were not redistributed, and the junctional H atoms were located on the C or N atoms, hence they originate. This procedure prevents the fragments from acquiring a non-net fractional charge because of the multipole redistribution. It also prevents any junctional atom or bond multipole from being at too short distances (<1 Å) from a polarizable centre belonging to an adjacent fragment. The total interaction energy was computed as the sum of intra- and intermolecular interfragment interactions computed simultaneously. To validate SIBFA, we perform parallel computations with both SIBFA and QC procedures on model complexes comprising the inhibitor, Zn(II), and PMI residues belonging to, or close to, the recognition site, as specified below. The values of SIBFA "intermolecular" interaction energies in the model binding sites were computed as the difference between such a summed energy and that of the ligand alone in the same geometry as in the corresponding complex. The intramolecular energy of the terminal end of each side-chain in these models was zero, since each consists of one single fragment.

Energy Minimizations

These were done with the Merlin package.[71] As reported in our previous studies,[51–53] the protein backbone was held rigid, and the side-chains of the residues in or in the immediate vicinity of the recognition site were relaxed. The six intermolecular variables defining the inhibitor orientation in its complexes and its torsion angles were relaxed, as well as the position of Zn(II). The orientation and conformation of the inhibitor were first minimized in the rigid enzyme by enforcing distance constraints between Zn(II) and the hydroxamate or carboxylate groups (modes *A or C*) or the phosphate (modes *B or D*). The constraints were then removed, and the side-chains torsion angles of relevant PMI residues were relaxed as well. These residues are: Trp18, Glu48, Phe99, Lys100, Ser103, Glu105, Lys106, Ser109, Gln111, His113, Asp115, Asn134, His135, Lys136, Glu138, Phe146, Glu147, Phe149, Cys150, Met277, Phe278, Gln280, Lys282, Asp283, His285, Tyr287, Ser289, Asp291, Glu294, Cys295, Met296, Ser299, Asp300, Asn301, Arg304, Phe307, Lys310, Phe311, Lys312, Asp313, Lys315, Asn316, Glu319, and Met320. These were selected on the basis of their being part of the PMI recognition site or their vicinity to it. They are all within 15 Å of Zn(II). Energy-minimizations were first performed in the absence of continuum reaction field effects and were resumed in their presence. Such explorations are limited to the sets of internal variables. This is certainly relevant, as we are interested in relative binding energies and that the inhibitors are built up with building-blocks with no internal strains and well-defined standard geometries.

In order to explore the energy surface with more details, we also performed another round of energy-minimizations. In these, the minima derived for PMI–5PAH complexes were used as a starting points for PMI–5PAA and conversely. Thus complexes *A* and *B* of 5PAH produced complexes *C′* and *D′* of 5PAA, respectively. Conversely complexes *C* and *D* of 5PAA produced complexes *A′* and *B′*, respectively, of 5PAH. Because *A′* had monodentate binding of hydroxamate to Zn(II) (see below), we have performed on it one more round of energy-minimization by enforcing bidentate binding, and then resuming after removal of the constraints. The corresponding complex is denoted *A′*. Uninhibited PMI was energy-minimized following replacement of the inhibitor by a water molecule in the Zn(II) binding site.

QC Computations

The *ab initio* computations used the coreless effective potential (CEP) 4-31G(2d) basis set developed by Stevens et al.,[72] which encompasses two 3d polarization functions on the heavy atoms, and the LACV3P** basis set, which is equivalent to the 6-311G** set on the nonmetal atoms.[73] The density functional theory (DFT) computations used the B3LYP[74,75] functional and the CEP 4-31G(2d) basis set as well as the LACV3P** basis set. The CEP 4-31G(2d) computations used the Gaussian 03,[76] and the LACV3P** ones used the Jaguar 6.0 software.[77] The Hartree–Fock (HF) and DFT methods in Jaguar use a pseudospectral method to compute the integrals.[78]

Calculation of Solvation Energies

We have resorted to two procedures. The first[64] is within the context of the Poisson–Boltzmann (PB) theory and is operational in the Jaguar 6.0 code. The molecular charge distribution is represented by a set of point charges on the atomic centers that are obtained by fitting the long-range Coulomb field from the quantum chemical wave function by least-squares. The reaction field produced by the solvent continuum is fit to another set of point charges, which are used to perform a new SCF calculation of the solute wave function in presence of the solvent point charges. The process is then reiterated until convergence of the solvation energy. Two additional contributions are included.

One, denoted as the reorganization energy, is the difference between the solute energy after the last iteration but without the solvent terms and its gas phase energy prior to PB computations. The other, denoted as a cavitation term, corresponds to the solvation energy of a nonpolar solute of identical size and shape as the solute considered. It is expressed as a linear function of the solute surface area.[64]

The second procedure is the PCM by Tomasi and Persico.[65] We have used the version coded in G03 with the default options.[76] ΔG_{solv}(PCM) has four contributions. The electrostatic term results from iterative coupling of the potential generated by the molecular wave function of the solute and the reaction potential and field of the bulk solvent on the solute surface. The repulsion and dispersion terms are computed following earlier formulations by Huron and Claverie.[62] A cavitation term is computed using the Pierotti formula.[63]

AMBER Molecular Dynamics

We used the polarizable ff03 force-field[79] of the AMBER 9.0 package.[80] Constant volume MD was performed at 300 K for a 1.2 ns length. Continuum solvation effects were computed using the MM/PBSA[81] model.

Results and Discussion

ΔG_{solv} *Computations of Representative Molecules*

For simplicity, we will denote by E_{reorg}(PB) and E_{cav}(PB) the reorganization and cavitation terms, respectively, whose formulations were integrated in the PB formalism. We will similarly denote by E_{rep}(PCM), E_{disp}(PCM), and E_{cav}(PCM), the repulsion, dispersion, and cavitation terms, respectively, that were integrated in the PCM formalism. The molecules reported in Table 1, which will be encountered in the model PMI complexes analyzed in the last section of this paper, belong to the following categories: (i) *polar*: water, formamide; (ii) *anionic*: formate, hydroxamate, and hydrogenophosphonate $(HPO_3)^{2-}$; (iii) *cationic*: methyl ammonium and Zn(II); (iv) *conjugated*: imidazole, indole, and benzene; and (v) *aliphatic*: methane. In addition, we include ΔG_{solv} of isolated 5PAH and 5PAA in their energy-minimized conformations in the presence of the continuum reaction field. We would like to comment on the following features, which will be important in the subsequent assessment of the LC *versus* PB or PCM approaches on the model PMI complexes, and for future refinements of the LC procedure.

ΔG_{solv} *Values*

As reported in Table 1, the values of ΔG_{solv}(LC) are in most cases close to those of ΔG_{solv}(PB) and ΔG_{solv}(PCM), the numerical agreement being generally better with ΔG_{solv}(PCM). One notable exception is water, for which the LC value of −4.9 kcal/mol is closer to the experimental value of −6.3 than the present PB ones (−9.4 and −8.1 kcal/mol at HF and DFT levels respectively) but less good than the −6.7 kcal/mol with PCM. For methylammonium, the LC value of −72.3 kcal/mol is intermediate between the PB and PCM ones of −79.5 and −65.2 kcal/mol respectively. For indole, the LC value of −3.6 kcal/mol is underestimated with respect to the −6.1 and −8.2 respective PB and PCM values. For both formohydroxamate and hydrogenophosphonate anions, the ΔG_{solv}(LC) values of −83.2 and −245.7 kcal/mol are much closer to the respective PCM ones of −81.6 and −246.4 kcal/mol than to the PB ones of −90.6 and −281.8 kcal/mol. Redoing ΔG_{solv}(PCM) calculations on formohydroxamate and hydrogenophosphonate with the

Table 1. Values (kcal/mol) of the Langlet–Claverie (LC), Poisson–Boltzmann (PB), and Polarizable Continuum Model (PCM) Solvation Energies and Their Contributions for Small Representative Molecules.

	Water	Formamide	Formate	Formohydroxamate	HPO_3^{2-}	Methyl ammonium	Zn(II)	Imidazole	Indole	Benzene	Methane	5PAH	5PAA
ΔG_{solv} (LC)	**−4.9**	**−13.0**	**−84.7**	**−83.2**	**−245.7**	**−72.3**	**−470.9**	**−11.4**	**−3.6**	**−0.7**	**1.2**	**−423.0**	**−406.8**
E_{el}	−5.2	−11.3	−83.1	−80.3	−245.2	−71.1	−473.8	−8.1	−3.4	−1.3	−0.2	−410.1	−395.2
E_{rep}	0.6	1.2	1.1	1.4	0.9	1.0	0.0	1.5	1.2	0.9	0.5	3.3	3.2
E_{disp}	−5.0	−9.8	−8.9	−11.4	−9.8	−8.8	0.0	−13.3	−14.4	−11.2	−5.2	−31.5	−30.3
E_{cav}	4.6	6.9	6.2	7.1	8.3	6.6	3.3	8.5	13.2	11.1	6.1	15.3	15.5
ΔG_{solv} (PB)[a]	**−9.4**	**−15.1**	**−82.2**	**−90.6**	**−281.8**	**−79.5**	**−480.4**	**−11.2**	**−6.1**	**−0.7**	**1.4**	**−436.0**	**−424.3**
E_{el}	−12.6	−20.6	−86.2	−99.4	−285.6	−82.6	−481.9	−16.8	−9.8	−3.2	−0.4	−451.4	−433.9
E_{reorg}	1.5	3.6	2.1	6.8	4.1	1.2	0.0	3.5	1.2	0.2	0.0	12.3	6.6
E_{cav}	1.7	2.0	1.9	2.0	2.0	1.9	1.6	2.2	2.6	2.3	1.8	3.0	3.0
ΔG_{solv} (PB)[b]	−8.1	−15.1	−78.9	−87.3	−280.3	−79.6	−480.3	−9.6	−5.0	0.1	1.4	−423.3	−419.3
ΔG_{solv} (PCM)[c]	**−6.7**	**−15.2**	**−82.6**	**−81.6**	**−246.4**	**−65.2**	**−474.2**	**−12.8**	**−8.2**	**−1.2**	**6.9**	**−416.0**	**−385.8**
E_{el}	−9.0	−18.1	−85.8	−84.8	−248.8	−70.2	−477.5	−16.1	−12.8	−5.1	−0.1	−425.2	−394.5
E_{rep}	0.5	0.7	0.8	0.8	0.9	0.4	0.0	0.9	1.4	1.0	0.1	1.7	−21.5
E_{disp}	−3.9	−7.1	−7.8	−7.8	−9.1	−6.0	0.0	−9.6	−14.7	−11.3	−3.1	−21.7	1.7
E_{cav}	5.7	9.3	10.2	10.2	10.6	10.6	3.3	12.0	17.9	14.2	10.0	29.2	28.5

[a]LACV3P** basis set, HF.
[b]LACV3P** basis set, DFT.
[c]CEP 4-31G(2d) basis set.

6-311G** basis set decreased by only −0.1 and −2.1 kcal/mol their ΔG_{solv} values. The 16.2 kcal/mol difference of ΔG_{solv}(LC) of 5PAH and 5PAA is closer to the 11.7 kcal/mol PB one than to the 30.2 kcal/mol PCM one.

Individual Contributions

The E_{el}(LC) contribution is in good correspondence with its PCM counterparts for ionic molecules. It is however underestimated with the present calibration in the case of polar and conjugated molecules. E_{rep}(LC) and E_{disp}(LC) have somewhat larger magnitudes than their PCM counterparts, but E_{cav}(LC) is systematically smaller, by factors of 1.2–1.9, than E_{cav}(PCM). With the default G03 options, E_{cav}(PCM) has an unexpectedly large value for methane (10 kcal/mol), resulting into an overestimated ΔG_{solv}(PCM) of 6.9 kcal/mol, while the experimental value is of 1.9 kcal/mol. The nonpolar PB contribution has in general small magnitudes, except for three anionic molecules where it is larger than 6 kcal/mol. E_{cav}(PB) has small values for all investigated molecules. Its magnitude is from threefold to tenfold less than E_{cav}(PCM), and from twofold to fivefold less than E_{cav}(LC). We also note that for the three water, formamide, and methane solutes, the values of the summed LC E_{disp} and E_{rep} contributions of −4.3, −7.6, and −4.7 kcal/mol, are in a range consistent with the corresponding available values reported in Table 10 in the 1994 review paper by Tomasi and Persico.[65]

Structural Aspects

Results from AMBER Molecular Dynamics

Figure 4 shows a superimposition of the main-chain of PMI as averaged on the one hand, from the AMBER MD trajectory, and as obtained on the other hand by high-resolution X-ray crystallography. There is a very strong overlap between the two structures. This should attest for the high stability of the backbone, and justify the use of a fixed backbone in the SIBFA energy-minimization. In the absence of explicit waters, a tetrahedral environment is found around Zn(II). The distances between Zn(II) and O, N, O, and N ligands of Gln111, His113, Glu138, and His285 are 1.8, 1.7, 2.1, and 2.0 Å, respectively. The corresponding distances obtained from X-ray crystallography are 2.15, 2.14, 2.15, and 2.08 Å, respectively. In Figures 5–9, we have modeled as a formamide-like entity the backbone segment between Leu108 (carbonyl) and Ser109 (amide). For conciseness, it was given the label "Leu108 (main)" in these figures.

Uninhibited PMI

At the periphery of the Zn(II)-binding site, there is an array of H-bonds involving in succession Glu48, Lys100, Glu294, and Tyr287. With water acting as an additional ligand (dZn—O = 2.2 Å), the distances between Zn(II) and the four coordinating PMI residues are close to their experimental counterparts. In addition, a fifth PMI residue, Tyr287, contributes to Zn(II) ligation through its phenolic O, but with an elongated Zn—O distance (2.5 Å, as opposed to 4.8 Å in the X-ray structure). The complex at the PMI recognition site is represented in Figure 5a. At the Zn(II) binding site, a good overlap can be seen between the energy-minimized and the X-ray structures, except for the location of Tyr287 and that of Lys310, which remains close to its position in inhibitor-bound PMI (Fig. 5b). Energy-minimization restarted from the experimental Lys310 side-chain torsion angles restored a similar conformation to that in Figure 5. This was driven principally by the electrostatic terms E_{MTP} and E_{pol}. These may drive Lys310 closer towards the centre of PMI on account of the net charge of −3.

PMI–5PAH Complexes

None of the inhibited PMI complexes investigated below has more than five Zn—O/N ligand distances < 2.5 Å. We report in Figures 6a–6c and 7a and 7b the 5PAH complexes in modes *A* and *B* respectively. The representation is limited to the PMI residues involved in inhibitor binding. Glu48, which accepts a proton from Lys100, was also included. It has been extended to

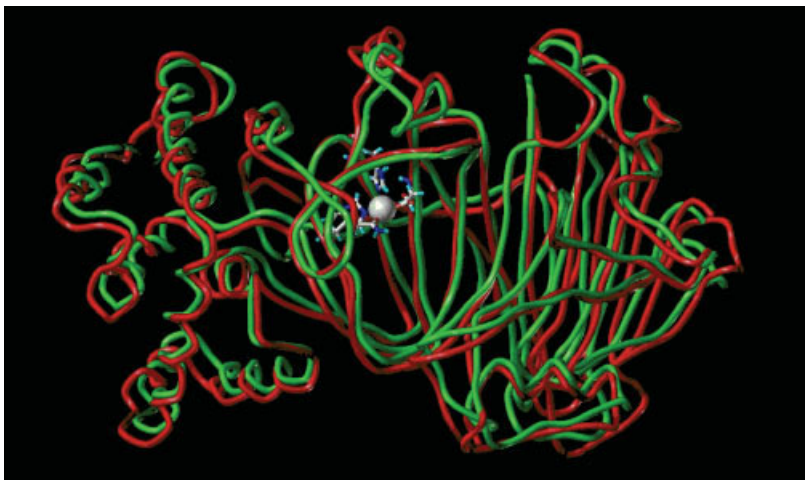

Figure 4. Superimposition of PMI main-chain (a) resulting from AMBER molecular dynamics and (b) obtained by high-resolution X-ray crystallography. [Color figure can be viewed in the online issue, which is available at www.interscience.wiley.com.]

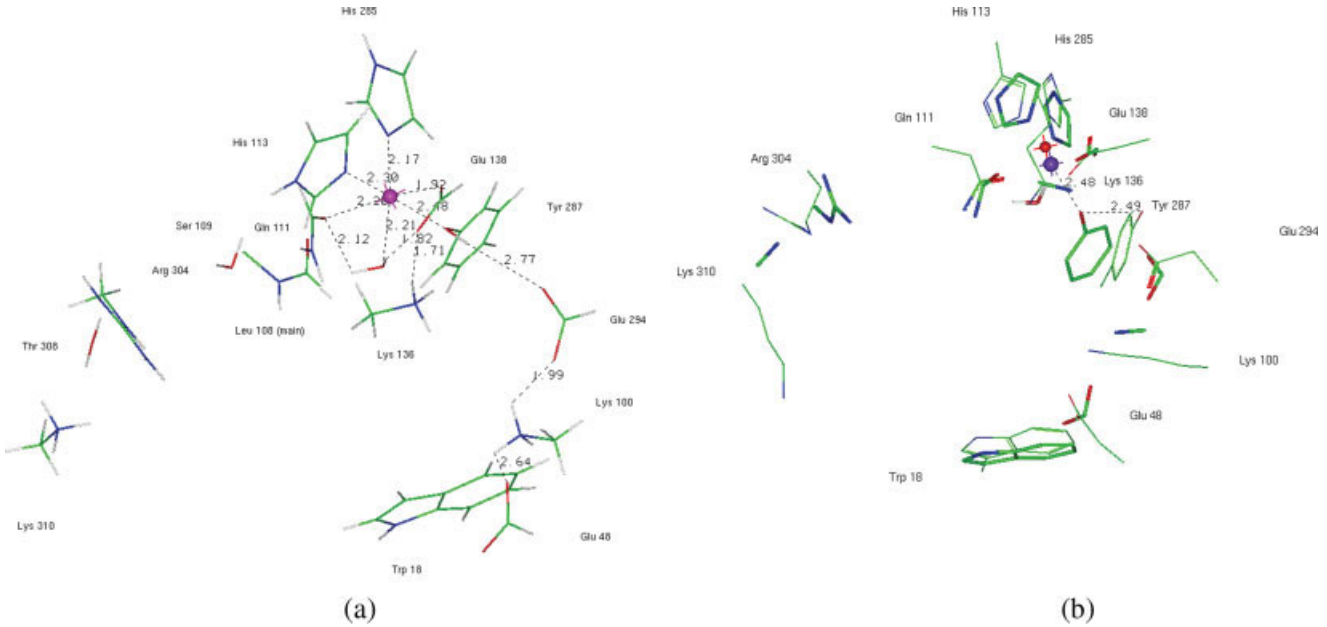

Figure 5. Representation of the inhibitor-free PMI recognition site, with one water replacing 5PAH in the Zn binding-site. (a) After SIBFA energy-minimization; (b) superimposition of the energy-minimized and of the X-ray structures. [Color figure can be viewed in the online issue, which is available at www.interscience.wiley.com.]

Trp18. This residue constitutes the "floor" of the recognition site. It was included to afford for more realistic LC *versus* QC comparisons of continuum solvation energies in the model sites by partly shielding the ligand from bulk solvation in such sites (see below). In addition, this residue constitutes a target for the design of novel 5PAH derivatives having aromatic lateral groups. The hydroxyl end of Thr308 side-chain has been included because of its vicinity to Arg304 and Lys310.

Modes A. In these modes, the hydroxamate moeity is complexed to the Zn(II) binding site, and the phosphate is in the vicinity of Arg304 and Lys310 at the entrance of the cavity. Mode A' results from an energy-minimization using the corresponding 5PAA minimum as a starting point. A'' results from an additional energy-minimization restarted from A' with hydroxamate bidentate binding to Zn((II) enforced in a first step, and relaxed in a second step. All three complexes have, similarly to uninhibited PMI, the Tyr287-Glu294-Lys100-Glu48 H-bonded array. In the first investigated mode *A*, the hydroxamate moiety binds in a bidentate fashion to Zn(II), the two Zn—O distances being 2.4 and 2.0 Å for the C- and N-connected oxygens, respectively (Fig. 6a). Bidentate binding occurs at the expense of the coordination of Zn to His285, the corresponding Zn—N distance being lengthened to 2.9 Å. Zn coordination is completed with His113, Glu138, and Gln111, the corresponding Zn-ligand distances being 2.2, 2.0, and 2.1 Å, respectively. At the entrance of the cavity, the phosphate group binds simultaneously, through two anionic oxygens, to Arg304 and Lys310, and through its third O, to Ser109. The fact that the phosphate group faces two monocationic residues appears to us as a strong argument in favor of a dianionic phosphate group. Furthermore, and considering that the pK_a 2 of the phosphate group (6.5) is close to the pH of the buffer we used for the kinetic analyses (7.1),[45] we assumed that the local pH at the active site is equal to the pH of the buffer because the active site of PMI is wide opened to the buffer. Hence, the charge of the phosphate is most likely −2. In all three modes *A*–A'', we observe that both Glu138 and Gln111 Zn(II) ligands interact, either directly, or indirectly, with 5PAH. Thus in mode *A*, the other Glu138 anionic O accepts a proton from Lys136, and this residue donates another proton to the 2-OH of 5PAH. The latter group in turn donates its proton to the vicinal 3-OH. Gln111 donates a proton to the 5PAH 4-OH group, which donates its own proton to the third phosphate oxygen. Such a pattern is also observed in modes A' and A''. In mode A' (Fig. 6b), the hydroxamate is bound monodentately to Zn(II) through its N-connected O (Zn—O distance = 2.0 Å), while both His113 and His285 now coordinate Zn(II), the two Zn—N distances being of 2.3 Å. Zn(II) coordination is completed with Glu138 and Gln111 with Zn—O distances of 2.0 and 2.1 Å, respectively. As in mode *A*, the phosphate group binds simultaneously to Arg304, Lys310, and Ser109. Glu138 accepts, through its second anionic O, a proton from Lys136, which donates another proton to the C-bound hydroxamate O, instead of the 2-OH as in mode *A*. Mode A'' has very similar Zn-coordination and H-bonding pattern as mode *A*, and differs essentially from it by the inclination of the Tyr side chain (Fig. 6c).

Modes B. In these modes, it is now the phosphate moeity that is complexed in the Zn(II) binding site, while the hydroxamate is in the vicinity of Arg304 and Lys310. Mode B' results from an energy-minimization using the corresponding 5PAA minimum as a starting point. In mode *B*, the phosphate group binds Zn(II)

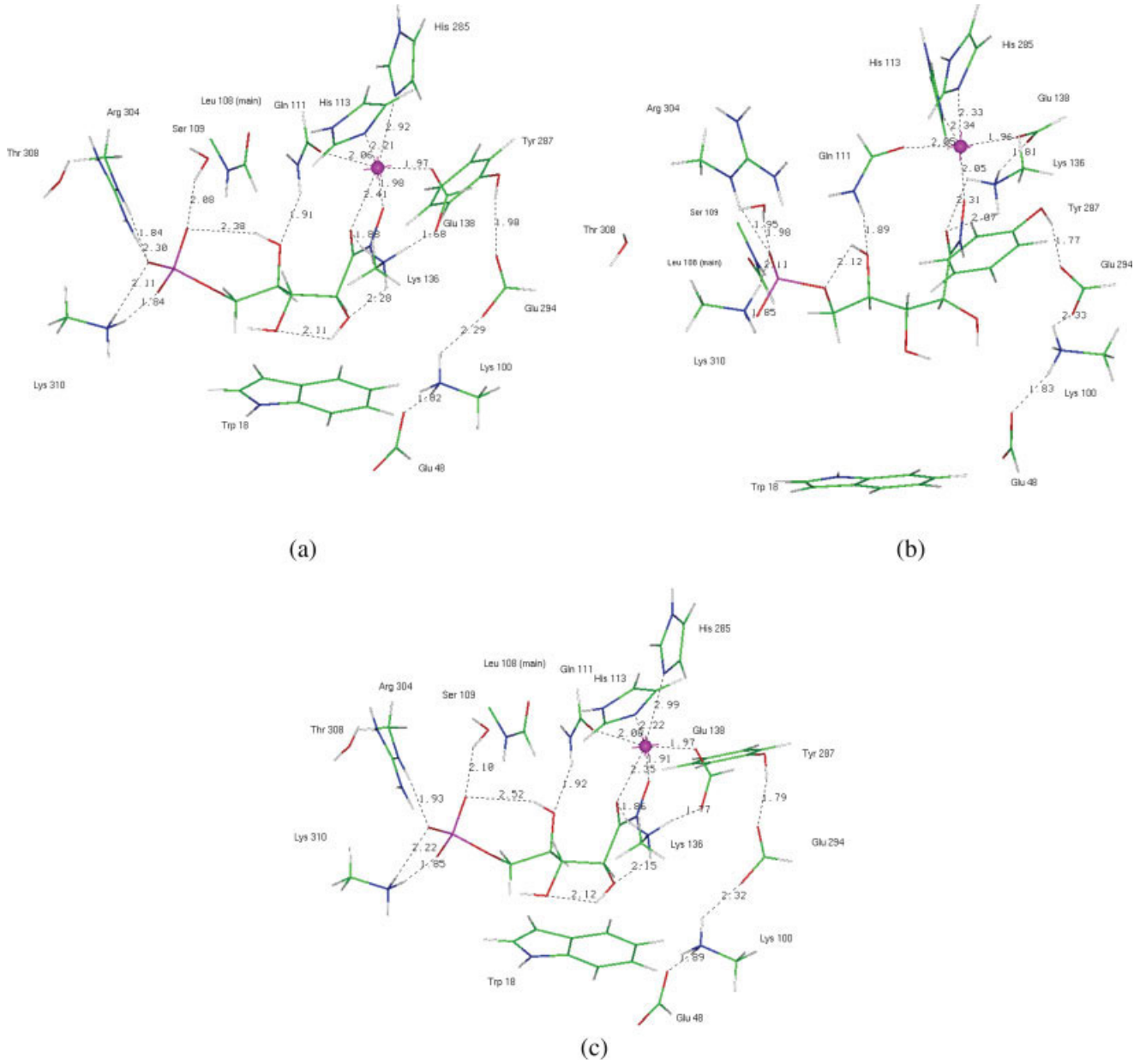

Figure 6. Representation of the 5PAH–PMI complex in modes *A*, showing only the PMI residues of the recognition site: (a) Mode *A*; (b) Mode *A′*; (c) Mode *A″*.

through two anionic oxygens, with Zn—O distances of 1.8 and 2.6 Å (Fig. 7a). This occurs at the expense of Zn-coordination by both His residues, the two Zn—N distances being >2.9 Å. While Glu138 remains coordinated to Zn(II), with a Zn—O distance of 1.9 Å, the Gln111-Zn distance has significantly increased (3.0 Å). The phenolic O of Tyr287 has entered the cation coordination sphere, the Zn—O distance being 2.1 Å. Glu138 accepts a proton from Lys136, which donates another proton to the phosphate, which also accepts a proton from Gln111. It also accepts, through its Zn-coordinating O, the Tyr287 phenolic proton. In complexes *A* (Fig. 6a), this proton was donated to the 4-OH group of 5PAH. In mode *B′* (Fig. 7b), the phosphate is no longer coordinated to Zn(II). The coordination of the cation to both His residues is restored, and a tetrahedral environment involving Glu138 and Gln111 is completed around it. The phosphate group has an ionic H-bond with Lys136. It also interacts with Gln111, but through two elongated distances between two anionic oxygens and one amide H. The hydroxamate group interacts simultaneously with both Arg304 and Lys310, but with a very short O—H distance to Lys310 of 1.5 Å. Such structural aspects lead to anticipate unfavorable binding energies for modes *B*.

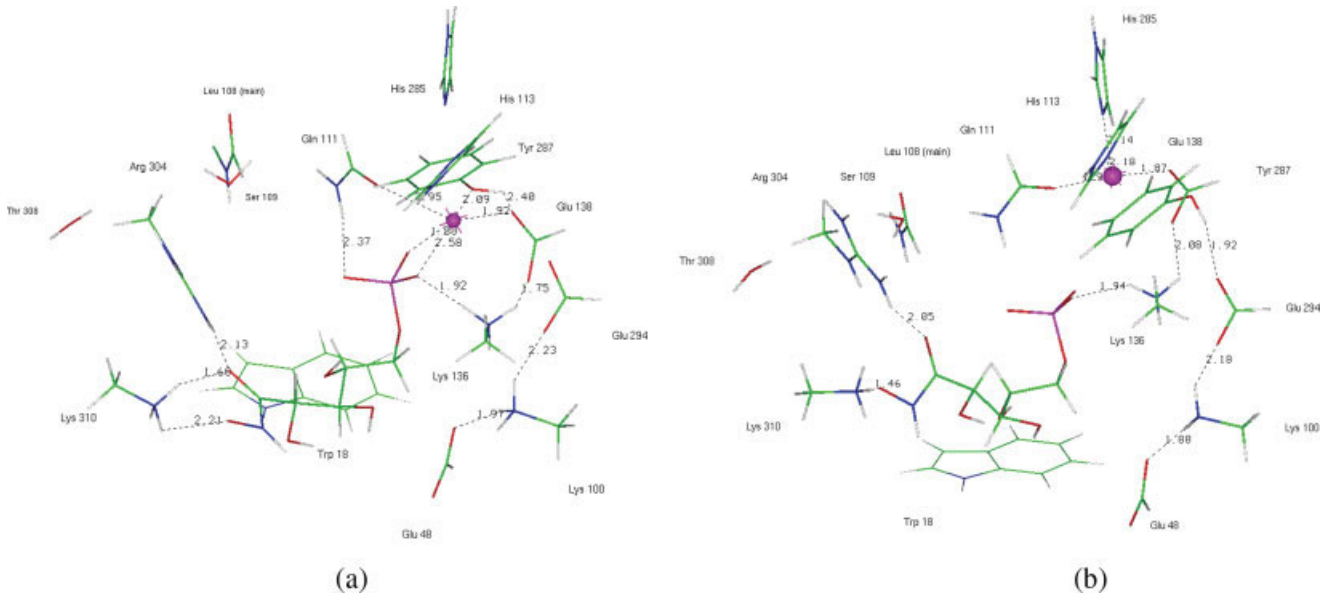

Figure 7. Representation of the 5PAH–PMI complex in modes *B*, showing only the PMI residues of the recognition site: (a) Mode *B*; (b) Mode *B′*. [Color figure can be viewed in the online issue, which is available at www.interscience.wiley.com.]

PMI–5PAA Complexes

We report in Figures 8a–8c and 9a and 9b the 5PAA complexes in modes *C* and *D,* respectively.

Modes C. In these modes, the carboxylate and phosphate moieties are complexed to, or in the vicinity of, the Zn(II) binding site, and to the Arg304–Lys310 site respectively. Mode *C′* results from an energy-minimization using the corresponding 5PAH minimum as a starting point. In mode *C* (Fig. 8a), the carboxylate group is bound monodentately to Zn(II). The Zn—N(His285) distance is again elongated ($d = 2.6$ Å). The Zn distances to the ligating atoms of Gln111, His113, and Glu138

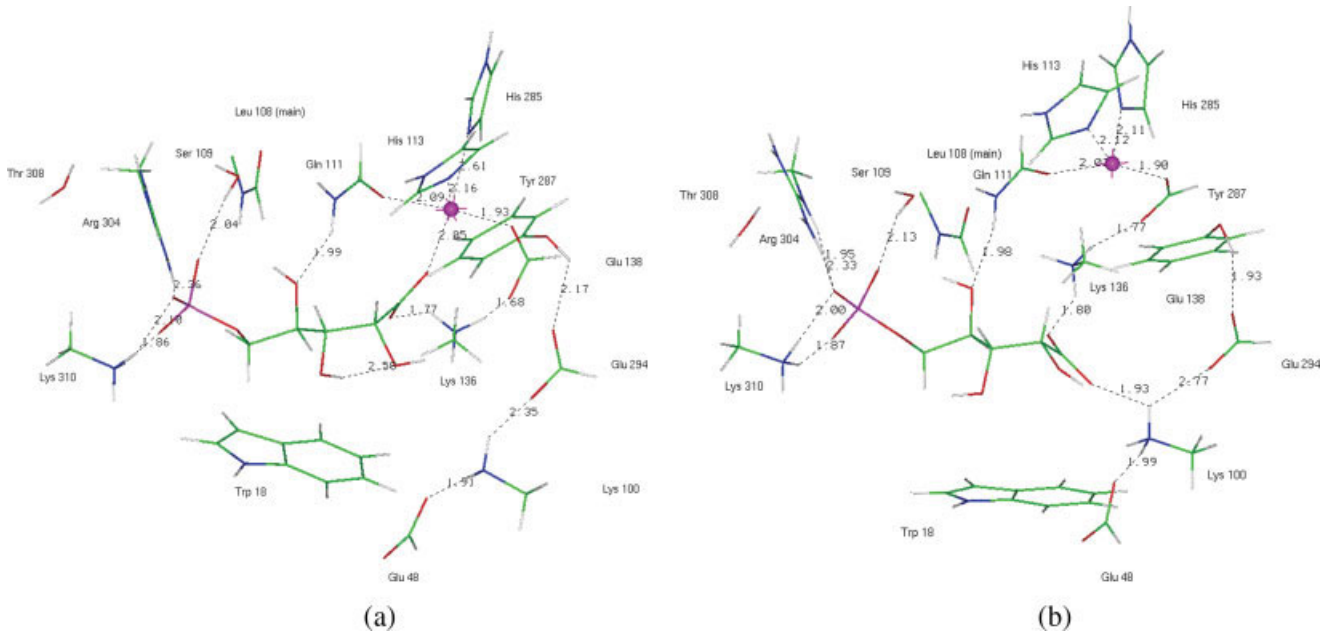

Figure 8. Representation of the 5PAA–PMI complex in modes *C*, showing only the PMI residues of the recognition site: (a) Mode *C*; (b) Mode *C′*. [Color figure can be viewed in the online issue, which is available at www.interscience.wiley.com.]

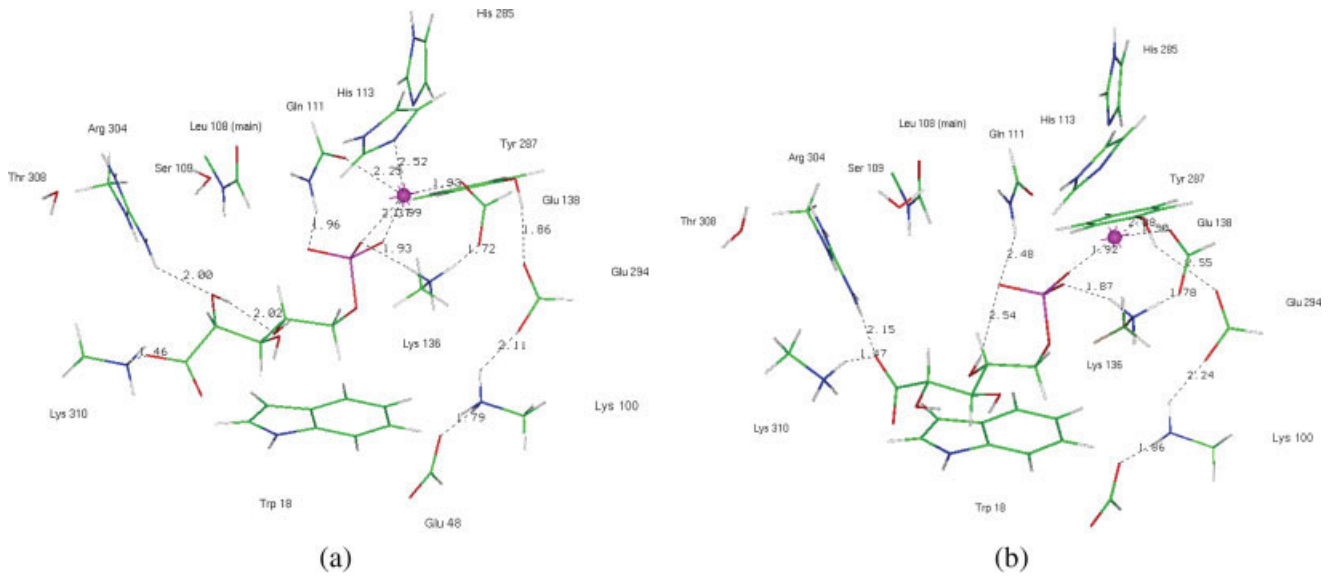

Figure 9. Representation of the 5PAA–PMI complex in modes *D*, showing only the PMI residues of the recognition site: (a) Mode *D*; (b) Mode *D*′. [Color figure can be viewed in the online issue, which is available at www.interscience.wiley.com.]

are similar to those in mode *A*′ (Fig. 6b). Similar to this mode, the non Zn-ligating anionic O of carboxylate accepts a proton from Lys136, which donates another proton to the non Zn-ligating anionic O of Glu138, and the 4-OH group accepts a proton from Gln111. As in modes *A* (Figs. 6a–6c), the phosphate group interacts through two anionic O's with both Arg304 and Lys310, and its third O accepts a proton from Ser109 side-chain. In *C*′ (Fig. 8b), the 5PAA carboxylate group no longer coordinates Zn(II). Instead, its anionic oxygens accept each one proton from the Lys100 and the Lys136 residues. Lys136 also donates a second proton to the non Zn-coordinating anionic O of Glu138, while Lys100 donates a second proton to Glu48. On the other hand, its distance to Glu294 is significantly elongated, the shortest H(N)—O distance being 2.8 Å instead of being in the range 2.3–2.4 Å. Zn(II) is fourfold coordinated. The reduction of coordination number results into shortened Zn distances (2.1 Å) to both His113 and His285 ligating N atoms. At the entrance of the cavity, the phosphate is bound simultaneously to Arg304, Lys310, and Ser109.

Modes D. In these modes, the phosphate is complexed to the Zn(II) binding site, and the carboxylate to the Arg304–Lys310 site. Mode *D*′ results from an energy-minimization using the corresponding 5PAH minimum as a starting point. In mode *D* (Fig. 9a), the phosphate is bound bidentately to Zn(II) (*d*Zn—O distances of 2.0 and 2.4 Å). One Zn-ligating O accepts an H from Lys136, which donates another proton to Glu138. The Zn-distance to its ligating N from His113 is elongated (2.5 Å) and Zn-coordination to His285 is lost. The third phosphate O accepts a proton from Gln111. One carboxylate O accepts a proton from Lys310 (*d*O—H = 1.46 Å), while the 2-OH group accepts a proton from one Arg304 cationic proton, and donates its H to the 3-OH group. In mode *D*′ (Fig. 9b), the phosphate is bound monodentately to Zn(II) (*d*Zn—O = 1.9 Å). It binds through a second O to Lys136, and through the third O to Gln111. The Zn(II) coordination is limited to 3, the other two ligands being one Glu138 anionic O and the Tyr287 hydroxyl O, with respective *d*Zn—O distances of 1.9 and 2.1 Å, respectively. The 5PAA carboxylate binds simultaneously, through the same O, to Arg304 and Lys310. As with mode *B*′ (Fig. 7b), the distance between this O atom and the nearest Lys310 proton is very short (1.46 Å) so that unfavorable binding energies could be expected.

Energetical Aspects

In this article, we wish to address the following issues regarding the preferential binding mode of both 5PAH and 5PAA inhibitors at the active site of PMI from *Candida albicans*.

i. To what an extent can polarizable molecular mechanics account for the preferential binding of 5PAH to the Zn(II)-binding site through its hydroxamate moiety (modes *A*) rather than through its phosphate moiety (modes *B*)? This issue can be compounded by the fact that phosphate bearing a net charge of −2 should give rise to a substantially more favorable electrostatic interaction with Zn(II) than hydroxamate, which bears a net charge of −1. The dicationic charge of Zn(II) is neutralized to only a limited extent by the anionic charge of a ligating Glu138 residue, since Glu138 is itself engaged in a short ionic H-bond with a neighboring Lys136 residue. On the other hand, the entrance of the binding cavity has two cationic residues, Arg304 and Lys310, and both will be complexed to the 5PAH moiety, phosphate or hydroxamate, that is not involved in Zn(II) ligation. While their two

monocationic charges could compete with the dicationic charge of Zn(II), such charges are more delocalized, hence less attractive electrostatic and polarization energies than with Zn(II). On the basis of such simple considerations, it is phosphate, rather than hydroxamate, that could be anticipated to be the preferred Zn(II)-binding ligand.

ii. How will the interaction energies and energy balances of 5PAA–PMI complexes compare to those of the 5PAH ones? Hydroxamate has a significantly stronger Zn-binding affinity than carboxylate. Thus using SIBFA, the energy-optimized values of Zn-formohydroxamate and Zn-formate amount to −439.3 and −391.1 kcal/mol, respectively, hence an energy difference of 48 kcal/mol. To what an extent would such a preference be maintained when each of these two moieties is integrated into a larger ligand, namely 5PAH or 5PAA, respectively, considering the restrictions imposed by their larger molecular structures and the onset of additional anchoring interactions involving the phosphate moiety?

iii. To complete the energy balances, it is necessary to include the solvation energies of the competing inhibitor-PMI complexes, such as by resorting to a Continuum reaction field procedure. What is the impact of ΔG_{solv} on the energy balances? Solvation effects are most effective on the accessible sites at the entrance of the cavity, namely at the Arg304–Lys310 site. In modes *A* with hydroxamate bound to the Zn(II) site, the two cationic charges could be neutralized to a large extent by the phosphate dianionic charge. Conversely, in modes *B*, such two residues would have their cationic charges much less efficiently neutralized by the single anionic charge of hydroxamate. As a result, the electrostatic potential exerted by the solute at the entrance of the cavity would be closer to that of a net positive charge in modes *B* and closer to neutral in modes *A*. This should result into modes *B* being significantly favored by the electrostatic contribution of ΔG_{solv} over modes *A*. Could this possibly result into an actual reversal of the preferences set by the intermolecular interaction energies $\Delta E_{int,}$ if ΔE_{int} were to actually favor modes *A*?

iv. As in our preceeding studies, we will perform validation calculations of SIBFA by parallel QC computations on model complexes obtained by extracting, from the inhibitor-PMI complexes, the inhibitor, Zn(II), and the relevant fragments of the PMI residues making up the recognition site. For that purpose, we perform single-point SIBFA computations on such complexes, along with parallel QC computations at the uncorrelated HF, and at the correlated DFT and MP2 levels. Which numerical agreement could be expected between the SIBFA and QC results?

Energy Balances for the PMI–5PAH and PMI–5PAA Complexes

The results are reported in Table 2, which gives the values of the interaction energies in the complexes of PMI with 5PAH and 5PAA and their individual contributions: electrostatic multipolar E_{MTP}, short-range repulsion E_{rep}, their sum denoting the first-order term E_1, polarization E_{pol}, charge-transfer E_{ct}, and dispersion E_{disp}. From each of these contributions, we further substract the corresponding values in the uncomplexed, Zn(II)-bound PMI, namely ΔE_{tot}/PMI and in the uncomplexed 5PAH or 5PAA ligands, namely ΔE_{tot}/lig. The latter three values were computed by separate energy-minimizations done on the uninhibited, Zn(II)-bound PMI, and on 5PAH or 5PAA ligands taken in isolation. The results from the substractions are given with the superscript a. The substracted values sum to ΔE_{tot}. We give similarly the values of ΔG_{solv} using the LC procedure, and the resulting values, $\Delta G_{solv}{}^{a}$, after substraction of the solvation energies of separately energy-minimized Zn(II)-bound uninhibited PMI and 5PAH or 5PAA ligands. We also subtract the continuum solvation of the water molecule that ligates Zn(II) in uninhibited PMI, namely −4.9 kcal/mol using the present calibration of the LC procedure (superscript ^{b}). We denote by δE_{fin} the resulting energy balance $\Delta E_{tot} + \Delta G_{solv}{}^{a,b}$.

PMI–5PAH. Table 2 shows that for the PMI–5PAH complex, modes *A* have considerably more favorable ΔE_{tot} values than modes *B*, in the 70–80 kcal/mol range out of 210–225. This preference originates predominantly from the summed first-order term E_1. We observe $E_{pol}{}^{a}$ to be actually destabilizing, as E_{pol} is less attractive than the sum of its values in isolated, energy-minimized Zn(II)-bound PMI and 5PAH or 5PAA ligands. This is a likely consequence of the excess of negative charges in the PMI-inhibitor complexes. Thus, the net charge of the 164-residue model of uncomplexed Zn(II)-bound PMI is −3, and it passes to −6 upon binding of the 5PAH or 5PAA ligands. Previous calculations on polycoordinated Zn(II) complexes[58,82] showed that E_{pol} can have diminished values when there is an excess of anionic over cationic charges, the field exerted by the anionic ligands increasingly shielding the one exerted by the dicationic charge of Zn(II). Such an effect should have closely comparable magnitudes in the 5PAH and 5PAA complexes. Therefore, further enlarging PMI to include more remote cationic residues and yield neutral complexes should not affect the relative binding affinities. In A'', $E_{rep}{}^{a}$ has a virtually null value. This could be due to a lesser compaction around Zn(II) than in uninhibited PMI. On the other hand, its $E_1{}^{a}$ value is close to that of its related complex *A*. The least positive E_{pol} value is found for B', in which Zn(II) and the phosphate group are separated from one another and interact only indirectly, through an array of H-bonded interactions involving Lys136 and Glu138. In this connection, several previous computations from one of our laboratories[58,83] show E_{pol} to preferentially favor indirect (such as water-mediated) over direct cation–anionic ligand binding. Opposing ΔE_{tot}, ΔG_{solv} and $\Delta G_{solv}{}^{a}$ favor modes *B* over modes *A*, but by amounts that do not enable to revert the ΔE_{tot} preferences. B' has a ΔE_{tot} that is higher than *B* by a very large magnitude (70 kcal/mol), but a ΔG_{solv} that is much more favorable (85 kcal/mol), owing to the separation of dicationic Zn(II) charge and the dianionic phosphate one.

Both *B* and B' have large positive summed δE_{fin} values implying unfavorable binding. By contrast, all *A* complexes have negative δE_{fin} values. Complex A' has the most favorable ΔE_{fin} value, imposed by ΔE_{tot}. This implies that 5PAH would bind Zn(II) monodentately, and that Zn(II) would preserve its coordination to Gln111, His113, Glu138, and His285, with only limited (0.2 Å) elongation of the Zn—N distances. It is also seen that despite their strong mutual overlap, *A* and A'' have differing ΔE_{tot} and ΔG_{solv} values, the balance favoring A''.

Table 2. Interaction Energies (kcal/mol) of the Bifunctional Inhibitors in their Two Competing Arrangements PMI: A–A″: 5PAH With Hydroxamate in the Zn-Binding Site; B–B′: 5PAH With Phosphate in the Zn-Binding Site; C–C′: 5PAA With Carboxylate in the Zn-Binding Site; D–D′: 5PAA With Phosphate in the Zn-Binding Site; E: Uninhibited Protein; F and G: Uncomplexed 5PAH and 5PAA Inhibitors, Respectively.

	PMI–5PAH					PMI–5PAA				PMI	5PAH	5PAA
	A	A′	A″	B	B′	C	C′	D	D′	*E*	F	G
E_{MTP}	−6936.8	−6946.8	−6901.1	−6906.4	−6758.8	−6805.5	−6810.7	−6823.6	−6810.3	−6882.5	214.2	216.1
E_{MTP}[a]	−268.5	−278.5	−232.8	−238.1	−90.4	−139.1	−144.3	−157.2	−143.9			
E_{rep}	6318.7	6331.9	6278.4	6353.7	6293.3	6263.8	6303.9	6359.5	6304.4	6061.5	217.8	204.8
E_{rep}[a]	39.4	52.6	−0.9	74.4	14.0	−2.5	37.6	93.2	38.1			
E_1	−618.1	−615.0	−622.7	−552.7	−465.5	−541.7	−506.8	−506.8	−505.9	−821.0	432.0	420.9
$\boldsymbol{E_1}$[a]	**−229.1**	**−226.0**	**−233.7**	**−163.7**	**−76.5**	**−141.6**	**−106.7**	**−63.9**	**−105.8**			
E_{pol}	−400.5	−414.1	−402.0	−401.9	−442.6	−389.9	−452.1	−422.8	−407.0	−409.7	−37.1	−24.8
E_{pol}[a]	46.3	32.7	44.8	44.9	4.2	44.6	−17.6	11.7	27.5			
E_{ct}	−59.5	−60.5	−59.5	−54.9	−46.2	−48.9	−54.9	−42.3	−45.2	−37.9	−3.6	−2.5
E_{ct}[a]	−17.9	−18.9	−17.9	−13.3	−4.7	−8.5	−14.5	−1.9	−4.8			
E_{disp}	−1830.6	−1831.1	−1822.5	−1827.1	−1812.0	−1806.8	−1815.0	−1818.5	−1812.9	−1768.5	−42.7	−39.8
E_{disp}[a]	−19.5	−20.1	−11.5	−16.0	−0.9	1.4	−6.8	−10.2	−4.6			
$\boldsymbol{\Delta E_{tot}}$	**−220.2**	**−232.3**	**−218.3**	**−148.1**	**−77.9**	**−104.1**	**−145.6**	**−64.3**	**−87.7**			
$\boldsymbol{\Delta G_{solv}}$	**−3248.5**	**−3250.0**	**−3257.4**	**−3266.8**	**−3351.3**	**−3311.6**	**−3292.1**	**−3262.5**	**−3286.7**	**−3030.4**	**−423.0**	**−406.8**
ΔG_{solv}[a,b]	199.9	198.5	191.1	181.6	97.1	120.7	140.2	169.8	145.6			
$\boldsymbol{\delta E_{fin}}$[c]	**−20.3**	**−33.8**	**−27.2**	**33.5**	**19.2**	**16.7**	**−5.4**	**105.9**	**57.9**			

[a]After subtraction of the uninhibited protein + isolated inhibitor corresponding energies.
[b]Taking into account the LC Continuum solvation energy of the Zn-ligating water molecule in uninhibited PMI.
[c]$\delta E_{fin} = \Delta E_{tot} + \Delta G_{solv}$[a,b].

PMI–5PAA. Table 2 shows the values of ΔE_{tot} to be considerably more favorable for carboxylate than for phosphate binding to Zn(II), consistent with the corresponding 5PAH results. Complex *C′* has a 22 kcal/mol lower δE_{fin} than *C*, due to its 42 kcal/mol more favorable ΔE_{tot}. Within the present approach, it has a small attractive δE_{fin} (−5.4 kcal/mol), while all other 5PAA complexes have positive δE_{fin} values. This could imply that 5PAA, if it were able to bind to PMI, would do so by not entering the Zn(II) coordination sphere. We note that of all *A–C* complexes, *C′* is the only one to have a negative (stabilizing) E_{pol}[a]. As with complex *B′* discussed above, this could be due to the separation between Zn(II) and the 5PAA carboxylate with indirect interactions taking place together through the array of ionic bonds with Lys136 and Glu138. The two *D* complexes have the most unfavorable δE_{fin} values of all 5PAH and 5PAA complexes. The fact that 5PAH in its *A* complexes has the most negative δE_{fin} values is fully consistent with the experimental observations.[45] Such quantities however result from differences between the large energy values, namely the individual contributions of ΔE_{tot} on the one hand, and of ΔG_{solv}, on the other hand. Such terms, even though they resort to the same distributed multipoles to compute electrostatics, nevertheless do not have the same accuracies as compared to QC computations, as will be shown below. Further refinements in the calculation of ΔG_{solv} will remain necessary. There are two additional reservations regarding the actual magnitudes of δE_{fin}. The first is the absence of entropy effects, such as those resulting from restrictions in rotations around single bonds of the ligand upon complex formation. Such are estimated to 1.5–2 kcal/mol, i.e. ∼10 kcal/mol for both 5PAH and 5PAA. The only entropy effects accounted for by the present treatment are those embodied in the computation of ΔG_{solv}. The second is due to the absence of discrete waters of solvation. In this connection, a recent MD study that was performed with one of our laboratories bore on the complexes of bis-phosphorylated inhibitors with the SH2 domain of growth factor receptor bound (Grb2) protein, a target for the design of potential anticancer agents (Leroux et al., submitted). The computations done in a water bath showed the persistence over up to 2 ns trajectories of only a limited number of water molecules in the immediate vicinity of inhibitor-protein binding. On the basis of these findings, we are developing a procedure that resorts to a recent integration of MD to SIBFA (Gresh et al., work in progress) to characterize the location and possible persistence of "discrete" water molecules at the sites of PMI-inhibitor binding. The results will be reported in due course. The present results are concerned with energy differences between competing complexes and should be meaningful.

Validation by Parallel QC Computations

It was essential to validate the accuracy of the SIBFA computations by performing parallel QC computations on relevant complexes. With the softwares available to us, QC computations are obviously intractable on the 164-residue model of PMI. They can be performed, however, on reduced models that, with present computational software, can total up to 200 atoms. We have therefore extracted from the energy-minimized PMI complexes *A–D* (Figs. 6–9, respectively), the following molecules or molecular fragments: (i) 5PAH or 5PAA and Zn(II), (ii) the end of

side-chains of Gln111, His113, Glu138, and His285, which constitute the Zn(II) binding site, (iii) the end of side-chains of Arg304, Lys310, Thr308, and Ser109, which constitute the cationic binding site at the entrance of the cavity, (iv) the end of side-chains of Tyr287, Glu294, Lys100, and Glu48, which form an array of H-bonded complexes close to, or involving, the Zn-ligating residue Glu138; they are augmented with the end of side-chain of Trp18, which constitutes the floor of the recognition site, (v) a formamide fragment, representing the backbone between Leu108 and Ser109. The model complexes with 5PAH and 5PAA total 140 and 138 atoms, respectively. We have performed single-point SIBFA and QC computations at both uncorrelated HF and correlated DFT and MP2 levels. The HF calculations used both the CEP 4-31G(2d) and the LACV3P** basis sets. The DFT computations were done with the LACV3P** basis set, and the MP2 computations with the CEP 4-31G(2d) basis set. The computations were done in the same way as in our previous computations on the complexes of metallo-β-lactamase model binding site with captopril and thiomandelate.[52] Thus, for each of the four complexes, the values of ΔE(SIBFA) and its contributions were computed by substracting from the total energy of the complex and corresponding contribution, those of the inhibitor, 5PAH or 5PAA, taken in isolation and in the corresponding conformation. The molecular entities of the PMI model binding site being all made out of one single fragment, their intramolecular energies are zero. The corresponding QC ΔE's were computed by substracting from the energy of the model complex, the corresponding energies of each of the individual molecules or molecular fragments making up the complex. Thus, ΔE encompasses the interaction of the PMI residues between themselves and with Zn(II) simultaneously with their interactions with 5PAH or 5PAA and the latters' interactions with Zn(II). We have also computed the values of ΔG_{solv} using the LC procedure and the corresponding ΔG_{solv} computed by solving the PB equation within the context of HF and DFT calculations, as well as by the PCM procedure.[64,65] The results of the computations are reported in Tables 3 and 4 concerning the ΔE_{tot} (SIBFA) and ΔG_{solv} calculations respectively.

Comparisons With Uncorrelated Calculations. Without the E_{disp} contribution, ΔE(SIBFA) reproduces the numerical values of ΔE(HF) with the CEP 4-31G(2d) basis set with a maximal error of 17 kcal/mol out of 1250, i.e. <1.5%. The trend in absolute values of ΔE as found by the two approaches is the following:

$$A' > A > A'' > C > B \geq B' > D' > C' > D \quad \text{HF, CEP 4-31G(2d)}$$

$$A' > A > A'' > C > B > D' > B' \geq C' \geq D \quad \text{SIBFA}$$

We thus observe the same ordering by both approaches, except for complex B', found by SIBFA to have a less favorable ΔE than D', while the HF computations give the reverse. The destabilization of complex B' could be due to the very short (1.47 Å) distance between one carboxylate oxygen and one Lys310 ammonium hydrogen. Such inversions involve energy differences of <10 kcal/mol ouf of 1200, i.e. <1%. The trend found by the LACV3P** computations is:

$$A' > A > A'' > C > B' \geq B > D' > C' > D \quad \text{HF, LACV3P**}$$

It is consistent with the CEP 4-31G(2d) basis set one, except this time for the reversal in B' versus B ΔE values. Nevertheless these inversions involve quantities even smaller than those found with SIBFA, namely 3 kcal/mol out of 1240. The ΔE(SIBFA) values differ from the ΔE(HF/LACV3P**) ones by larger quantities than with the CEP 4-31G(2d) basis set (8–42 kcal/mole out of 1250, i.e., <3.5%), but if we except again complex B', have the same trends. A graph displaying the evolutions of ΔE(SIBFA) and ΔE(HF) for the *A–D* complexes is given in Figure 10.

The preference in favor of *A* complexes is clearly due to the first-order contributions E_1, and stems within E_1 from the electrostatic term E_{MTP}. For the other complexes, mutual interplays of first- *versus* second-order terms modulate the energetical orderings. This is the case for complex *C*, which ranks fourth in the series. Its preference over *B* is due to E_{pol}, while E_{ct} and, to a lesser extent E_1 favor *B* over *C*. Such a preference of E_{pol} could be due to a lesser shielding of the Zn(II) dipositive charge by the carboxylate than by the phosphate in these respective complexes. Complex C' ranks penultimate in the series, owing to its least stabilizing E_1. It has, conversely, the most favorable value of E_{pol}. This is likely due to the indirect Zn(II)-carboxylate interaction that is mediated through the Lys136–Glu138 ionic interactions (Fig. 8b). It is favored over *D*, the least stably bound complex, by E_{pol} and E_{ct} which overcome the inverse trend by E_1. At this point we would like to note that a single-point SIBFA computation on the 140-atom model complexes requires about 0.5 s of CPU time on a single sp5 IBM processor. The corresponding HF computation using Jaguar 6.0 requires 8 h, whence a ratio of about 60,000 in relative speeds. As previously mentioned,[58] this implies that SIBFA would be considerably faster than QM/MM procedures.

The value of ΔE(SIBFA) in the model for uninhibited PMI, in which 5PAH or 5PAA were replaced with water (last column of Table 3) is also very close to the ΔE(HF) ones. The relative error with respect to ΔE(HF/CEP4-31G(2d)) is 1%, similar to the ones found in the 5PAH and 5PAA complexes. This is certainly noteworthy, considering the fact that one small neutral ligand, namely water, has taken the place of large, trianionic ligands, resulting into an actual 2- to 2.2-fold drop in the magnitudes of ΔE.

Comparisons with Correlated Results. Passing to the DFT level enables to quantify the gain in interaction energy due to correlation. The interactions occurring in the 138- to 140-atom model complexes *A–D* do not involve actual "van der Waals" or apolar effects and are virtually only of cation-ligand and hydrogen-bonded types. For both kinds of interactions, close correspondences between ΔE(DFT) and ΔE_{tot}(SIBFA) (augmented with E_{disp}) have previously been demonstrated,[55,83–85] and such comparisons should be meaningful for the present complexes *A–D* as well. The SIBFA and DFT orderings are:

Table 3. Interaction Energies (kcal/mol) of the Bifunctional Inhibitors in the Model Binding Site Consisting of 14 Residues (See Text) Extracted From Their PMI Complexes in the Two Competing Arrangements: *A*–*A*″: 5PAH With Hydroxamate in the Zn-Binding Site; *B*–*B*′: 5PAH With Phosphate in the Zn-Binding Site; *C*–*C*′: 5PAA with Carboxylate in the Zn-Binding Site; *D*–*D*′: 5PAA With Phosphate in the Zn-Binding Site; *E*: Unligated PMI With One Water Molecule Replacing the Inhibitor in the Zn(II) Coordination Sphere.

	PMI-5PAH					PMI-5PAA				PMI
	A	*A*′	*A*″	*B*	*B*′	*C*	*C*′	*D*	*D*′	*E*
E_{MTP}	−1396.2	−1417.3	−1383.8	−1377.1	−1341.9	−1359.9	−1300.7	−1353.3	−1367.4	−625.6
E_{rep}	270.3	270.5	261.4	269.9	264.5	254.6	266.7	284.8	277.7	170.6
E_1	−1125.9	−1146.7	−1122.4	−1107.2	−1077.4	−1105.3	−1033.0	−1068.5	−1089.7	−454.9
E_{pol}	−122.0	−123.4	−122.8	−89.2	−113.7	−122.8	−147.5	−113.5	−102.5	−110.4
E_{ct}	−40.0	−40.7	−40.2	−46.5	−33.5	−39.8	−42.5	−40.0	−39.2	−30.9
ΔE	**−1287.9**	**−1310.8**	**−1285.4**	**−1242.9**	**−1224.6**	**−1267.9**	**−1224.0**	**−1222.0**	**−1231.4**	**−596.3**
ΔE[a]	**−1283.6**	**−1310.8**	**−1278.2**	**−1243.2**	**−1240.4**	**−1250.7**	**−1227.5**	**−1221.0**	**−1233.7**	**−601.6**
ΔE[b]	**−1315.0**	**−1344.9**	**−1308.6**	**−1264.9**	**−1266.1**	**−1278.7**	**−1252.0**	**−1242.4**	**−1256.6**	**−618.8**
E_{disp}	−86.1	−87.0	−85.4	−79.0	−76.5	−79.6	−78.4	−78.5	−76.6	−57.3
ΔE_{tot}	**−1374.0**	**−1397.8**	**−1370.8**	**−1321.9**	**−1301.1**	**−1347.5**	**−1302.4**	**−1300.5**	**−1308.0**	**−653.6**
ΔE(DFT)[c]	**−1358.5**	**−1386.9**	**−1349.8**	**−1295.1**	**−1300.9**	**−1324.2**	**−1295.4**	**−1288.0**	**−1299.9**	**−653.0**

[a]CEP 4-31G(2d) basis set.
[b]LACV3P** basis set, HF.
[c]LACV3P** basis set, DFT.

$$A' > A > A'' > C > B > D' > C' \geq B' \geq D \quad \text{SIBFA}$$

$$A' > A > A'' > C > B' \geq D' > C' \geq B \geq D \quad \text{DFT}$$

Although there are apparent inversions in the ordering of the last four complexes, while only *B*′ was misrepresented by SIBFA at the HF level, these stem from ΔE(DFT) differences of only 5 kcal/mol out of 1300 between them, namely <0.5%. Nevertheless it remains likely that some difficulty into more

Table 4. Values of the Solvation Energies (kcal/mol) and Their Contributions in the Complexes of the Bifunctional Inhibitors in the Model Binding Site Consisting of 14 Residues (See Text) Extracted From Their PMI Complexes in the Two Competing Arrangements: *A*–*A*″: 5PAH With Hydroxamate in the Zn-Binding Site; *B*–*B*′: 5PAH With Phosphate in the Zn-Binding Site; *C*–*C*′: 5PAA With Carboxylate in the Zn-Binding Site; *D*–*D*′: 5PAA With Phosphate in the Zn-Binding Site; *E*: Unligated PMI With One Water Molecule Replacing the Inhibitor in the Zn(II) Coordination Sphere.

	PMI-5PAH[ab]					PMI-5PAA[c,d]				PMI[e]
	A	*A*′	*A*″	*B*	*B*′	*C*	*C*′	*D*	*D*′	*E*
ΔG_{solv} (LC)	**−249.7**	**−251.6**	**−257.8**	**−280.9**	**−316.4**	**−264.5**	**−295.1**	**−275.1**	**−273.4**	**−521.8**
E_{el}	**−179.2**	**−180.0**	**−186.9**	**−210.3**	**−243.5**	**−193.2**	**−221.4**	**−205.6**	**−203.2**	**−468.3**
E_{rep}	16.5	16.3	16.5	16.5	17.1	16.4	16.6	16.6	16.4	14.3
E_{disp}	−149.5	−148.4	−150.3	−149.5	−155.2	−148.7	−150.9	−150.9	−148.3	−129.4
E_{cav}	62.6	60.5	62.8	62.4	65.2	61.0	60.6	64.7	61.7	61.7
ΔG_{solv} (PB)[a]	**−209.2**	**−207.8**	**−219.5**	**−254.1**	**−283.2**	**−221.1**	**−244.9**	**−237.4**	**−236.1**	**−481.3**
E_{el}	**−244.3**	**−243.2**	**−256.2**	**−299.3**	**−329.6**	**−257.7**	**−283.9**	**−275.6**	**−276.9**	**−519.3**
E_{reorg}	27.2	27.5	28.7	37.0	38.4	28.7	31.1	30.2	32.9	29.8
E_{cav}	7.9	7.8	7.9	7.8	8.0	7.9	7.9	8.0	7.8	8.0
ΔG_{solv} (PB)[b]	−186.8	−186.1	−196.0	−224.2	−255.8	−198.4	−219.9	−213.3	−210.3	
ΔG_{solv} (PCM)[c]	**−125.0**	**−133.1**				**−132.7**	**−162.0**			
E_{el}	**−214.8**	**−224.0**				**−224.9**	**−255.2**			
E_{rep}	6.0	6.0				5.8	5.8			
E_{disp}	−72.5	−73.1				−71.0	−71.3			
E_{cav}	156.3	158.0				157.4	158.7			

[a]LACV3P** basis set, HF.
[b]LACV3P** basis set, DFT.
[c]CEP 4-31G(2d) basis set.

accurately computing ΔE_{tot}(SIBFA) for complexes B' and D' could be due to the very short distance (1.46 Å) between one Lys310 ammonium proton and one anionic O of hydroxamate or of carboxylate, respectively. The absolute values of ΔE_{tot} (SIBFA) are larger than those of ΔE(DFT). This is fully consistent with the results from related comparisons done on the complexes of captopril and thiomandelate mercaptoxamide inhibitors with models of the binuclear Zn-metalloenzyme β-lactamase.[52] A graph displaying the evolutions of ΔE_{tot}(SIBFA) and ΔE(DFT) for the *A–D* complexes is given in Figure 10. Computations of ΔE(MP2) will not be reported in the present work because of the excessive CPU time required for all 10 complexes of Table 3. Previous comparisons between ΔE_{tot}(SIBFA) and ΔE(MP2) done with the above-mentioned models of the Zn-metalloenzyme β-lactamase had shown close agreements of SIBFA and MP2, the numerical values of ΔE_{tot}(SIBFA) being intermediate between the MP2 and the DFT ones, and the trends virtually parallel in twenty investigated complexes.[52] Finally the value of ΔE_{tot}(SIBFA) for uninhibited PMI is virtually identical (−653.6 kcal/mol) to its ΔE(DFT) counterpart.

Computation of Solvation Effects. Table 4 gives the values of ΔG_{solv} and their contributions for the LC, PB, and PCM approaches. In its present formulation and calibration, ΔG_{solv}(LC) has larger magnitudes than its PB counterparts at the HF and DFT levels. The relative errors of 20% with respect to the HF computations are obviously much larger than for the ΔE computations. On the other hand, such errors are fairly constant for the 10 investigated complexes. The orderings of ΔG_{solv}(LC) and ΔG_{solv}(PB/HF) values are, respectively:

$$B' > C' > B > D \geq D' > C > A'' > A' \geq A \quad \text{LC}$$

$$B' > B > C' > D \geq D' > C > A'' > A \geq A' \quad \text{PB/HF}$$

With the exception of complex C', the complexes with the most favorable ΔG_{solv} are those having either the hydroxamate or the carboxylate group, rather than the phosphate, at the entrance of the cavity. As mentioned above, for such complexes the two cationic charges of Arg304 and Lys310 are less shielded by the monoanionic hydroxamate or carboxylate charge than by the dianionic phosphate charge as is the case of complexes of types *A* or *C*. The electrostatic potential exerted on bulk solvent in complexes B–B' or D–D' should be accordingly stronger, whence a more favorable E_{el} contribution to ΔG_{solv}. In C', on the other hand, the dipositive charge of Zn(II) is, together with B', the least shielded in all inhibited model complexes because no direct Zn(II)-inhibitor interaction occurs in B' and C'. Such a feature should enhance ΔG_{solv} and it is observed that those two complexes rank amongst the three most favorable complexes in the *A–D* series. Interestingly, upon passing from the small model complexes of Tables 3 and 4 to the actual PMI ones of Table 2, we observe that while B' remains the complex with the most favorable ΔG_{solv}(LC), C' now has a lesser ΔG_{solv}(LC) than *C*. This could be due to the fact that the Zn(II) binding site being less accessible in the PMI model, reduced Zn(II) charge shielding in C' should have a lesser impact than maintenance of a net monopositive charge at the entrance of the cavity.

Comparing the trends of ΔG_{solv}(LC) and of ΔG_{solv}(PB), we observe one major inversion that occurs between the *B* and the C' complexes, with ΔG_{solv}(LC) favoring C' while ΔG_{solv}(PB) conversely favoring *B*. The energy differences amount to 14 kcal/mol out of 280, i.e. 5% in relative errors. There is one minor inversion occurring between *A* and A', but it involves energy differences of 2 kcal/mol out of 210. Computations with PCM were converged for only four complexes but indicated similar qualitative trends as for the LC procedure. We also report in Table 4 the values of individual contributions of ΔG_{solv} in the different approaches. It is clearly seen that it is E_{el} that imposes the ranking of ΔG_{solv} values and is responsible for the C' *versus B* inversion that occurs with the LC computations. To within 2 kcal/mol, the sum of E_{rep}(LC) + E_{disp}(LC) is flat except for complex B', which is favored by it by 4–5 kcal/mol out of 130 with respect to the other complexes. On the other hand, E_{cav} is also largest in complex B'. This results into the

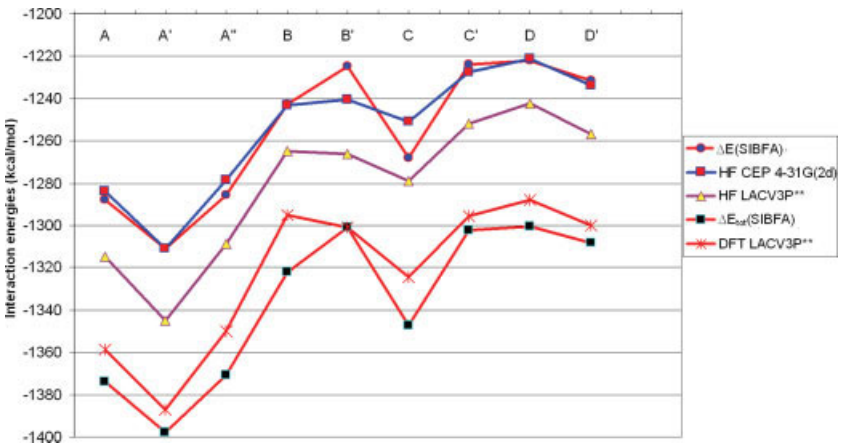

Figure 10. Evolutions of ΔE(SIBFA), ΔE(HF), and ΔE(DFT) in the *A–D* complexes of 5PAH and 5PAA in the model binding sites. [Color figure can be viewed in the online issue, which is available at www.interscience.wiley.com.]

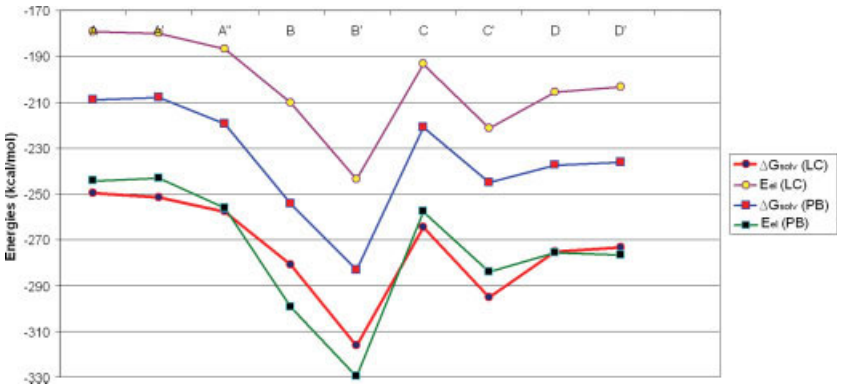

Figure 11. Evolutions of ΔG_{solv}(LC), ΔG_{solv}(PB), ΔG_{solv}(PCM), and their electrostatic contributions in the *A–D* complexes of 5PAH and 5PAA in the model binding sites. [Color figure can be viewed in the online issue, which is available at www.interscience.wiley.com.]

sum of all three nonelectrostatic terms having variations contained to 3.3 kcal/mol out of 70 for the nine complexes. E_{reorg}(PB) which is repulsive is largest for *B* and *B′* complexes. This is not in agreement with the behavior of E_{rep}(LC) nor of E_{rep}(LC) + E_{disp}(LC). E_{cav}(PB) has no variations in the nine complexes and as with the small molecule results is considerably smaller than E_{cav}(LC). The values of ΔG_{solv}(PB) at the DFT level are by about 20 kcal/mol smaller than at the HF level, but they run parallel to them. The trends in ΔG_{solv}(LC) and ΔG_{solv}(PB) and their E_{el} contributions are reported in Figure 11.

E_{el}(PCM) favors *A′* over *A*, but by a much larger amount (9.2 kcal/mol) than E_{el}(LC) (0.8 kcal/mol), while as mentioned above E_{el}(PB) favored *A* over *A′* by 1.4 kcal/mol. On the other hand, E_{el}(PCM) favors *C* over *A′* by a very small amount (0.9 kcal/mol), while the corresponding E_{el}(LC) and E_{el}(PB) differences are 13.2 and 14.5 kcal/mol, respectively. E_{rep}(PCM) and E_{disp}(PCM) are smaller in magnitude than their LC counterparts. We note in particular that E_{disp}(PCM) is about 2.1-fold smaller than E_{disp}(LC). The corresponding ratio never exceeded 1.5 in the small molecule computations reported in Table 1. On the other hand, E_{cav}(PCM) which varies very little is about 2.5 larger than E_{cav}(LC). The largest corresponding ratio in the small molecule computations was 1.8.

Two means to improve the match between ΔG_{solv}(LC) and its QC counterparts could be considered. One is to further modify the calibration of E_{disp}(LC) and E_{rep}(LC) in order to get improved matches with their PCM counterparts for ΔG_{solv} computations on both small molecules and model complexes such as *A–D*. The present analysis shows however that this should little affect the ΔG_{solv}(LC) *versus* ΔG_{solv}(PB) or ΔG_{solv}(PCM) trends which are clearly imposed by the E_{el} contributions. Thus the second means is to refine the computations of E_{el}(LC). We have towards this aim included an option that iteratively includes the contributions to the solute electrostatic potential of the dipoles induced on it by the reaction field of the solvent. However this was found to necessitate, in highly charged complexes, to search for a proper screening of the solute electrostatic field, similar to the one done for the E_{pol}(SIBFA) contribution (Langlet et al., in progress). Its inclusion was thus not done in the present study. We are presently investigating the possibility of accounting for the effects of charge redistribution in all molecular fragments after complex formation has taken place. In inter- or intramolecular computations, the energetical impact of charge redistribution is accounted for by E_{pol}(SIBFA) and E_{ct}(SIBFA) in which electrostatics resort to the permanent multipoles and induced dipoles. To compute the electrostatic potential sensed by bulk solvent, accounting in addition for charge redistribution could be necessary, particularly in the vicinity of a partially exposed dicationic charge as is the case for model complexes *A–D*. We are presently investigating procedures to include such effects that originate from polarization as well as from charge-transfer effects (Gresh et al., in progress). It is noted that to our knowledge, such effects are present so far in none of the molecular mechanics procedures currently in use to compute ΔG_{solv}, whether by Poisson–Boltzmann or by Generalized Born methods.

Conclusions

The final interaction energies ΔE determined for the two bifunctional inhibitors in their two competing arrangements with PMI allow us to address issues (i)–(iv) that were raised upon considering the energetical aspects of 5PAH *versus* 5PAA binding to PMI.

i. The 5PAH has a very strong preference in favor of hydroxamate rather than phosphate binding to Zn(II). This result is consistent with a catalytic role for the metal cofactor. Zn(II) coordination remains limited to 5. Thus hydroxamate can bind either bidentately to Zn(II), but at the expense of Zn(II) coordination to His285 (complexes *A* and *A″*), or monodentately, with limited elongations (up to 2.34 Å) of the Zn distances to the coordinating N of His113 and His285 residues (complex *A′*). The energy balances favor complex *A′*. Phosphate binding to Zn(II) results into a loss of Zn(II) coordination to both His113 and His285 (complex *B*). An alternative complex, denoted *B′*, in which phosphate is bound indirectly to Zn(II) through Lys136 and Glu138, was in fact found to be more stable than *B*.
ii. A much more stable complex was obtained in the case of 5PAH than for 5PAA, in accord with the inhibition properties reported for these molecules towards yeast and *P. aeru-*

ginosa PMIs. Indeed, binding affinity of 5PAA on PMI from *C. albicans* is not known. However, we have determined its binding affinity on PMI from yeast, also a type I PMI. Because all PMIs of this type share a strong homology, the IC_{50} value, we determined for 5PAA on yeast PMI gives us an estimation of the IC_{50} value on *C. albicans* PMI. The value we determined, 3.6 mM, compared to a K_m value of 0.12 mM, indicates that 5PAA is a weak PMI inhibitor. Comparatively, we had reported an IC_{50} value of 136 nM (0.136 μM) for 5PAH. These experimental results give us a value for the difference in free energy of 6 kcal/mol. In Table 2, we report a higher theoretical difference of free energies that is nevertheless fully consistent with the weak and strong binding affinities of 5PAA and 5PAH, respectively, towards PMI. With the PMI model, the differences in ΔE_{tot} values between complexes A–A'' and C were much larger than the sole differences of Zn(II)-hydroxamate *versus* formate interaction energies. In fact, and similar to model B', the best 5PAA complex, denoted as C', has its carboxylate indirectly bound to Zn(II) through Lys138 and Glu138.

iii. In the 5PAH complexes, ΔG_{solv} was in favor of phosphate binding to Zn(II). Direct binding (B) was much less favored than indirect binding (B'). ΔG_{solv} could not reverse the preferences set by ΔE_{tot} in favor of complexes A. In the 5PAA complexes, by contrast, ΔG_{solv} does not favor phosphate binding to Zn(II).

iv. Upon computing the intermolecular interaction energies in the nine model complexes, very close numerical agreements were found between SIBFA and QC computations. With respect to the CEP 4-31G(2d) basis set at the HF level, the maximum relative error in intermolecular interaction energies was less than 1.5%. The SIBFA interaction energies had trends that paralleled those of their QC counterparts, at both uncorrelated and correlated levels. Similar agreements have been previously demonstrated in complexes of mercaptocarboxamide inhibitors with models of a binuclear Zn(II) enzyme β-lactamase.[52] ΔG_{solv}(LC) had on the other hand much larger numerical deviations with respect to ΔG_{solv}(PB). Nevertheless it gave consistent trends in its variations for the nine investigated complexes, with only one major inversion that involved energy differences amounting to 5% of ΔG_{solv} values. Analysis of the individual contributions suggested that one possible refinement would bear on the electrostatic contribution of ΔG_{solv}(LC) by accounting for the effects of charge redistribution that take place upon complex formation.

Complexes A–A'' of PMI with 5PAH, where hydroxamate binds to Zn(II), were those yielding the most negative (stabilizing) δE_{fin} values. In fact, all other 5PAH or 5PAA complexes gave rise to positive δE_{fin} values, excepting complex C' of 5PAA, that had a small stabilizing (−5.4 kcal/mol) δE_{fin} value. The large absolute values of δE_{fin} derived for complexes A–A" result from mutual compensations of very large quantities, ΔE_{tot} and ΔG_{solv}, are in the −20 to −30 kcal/mol range and are overestimated. Entropic effects could reduce by ~10 kcal/mol the absolute values of δE_{fin} and bring it closer to values corresponding to ligands with nanomolar affinities (the only entropic effects included in the present treatment are those embodied in ΔG_{solv}). However, within the present approach, an important step towards more accurate assesments of the absolute magnitudes of δE_{fin} should await refinements in the Continuum procedure. An additional refinement would consist into inclusion of discrete waters in the immediate vicinity of inhibitor-PMI interaction sites, and monitor their time-dependent evolutions using the recent integration of MD to SIBFA. Finally, the most stable theoretical complex we obtained with 5PAH can allow us to propose the first hypothesis of a detailed view of the active site of the zinc PMI complexed to the high-energy intermediate analogue inhibitor 5PAH, with Lys136 and Glu138 as good candidates for the active site residues involved in the proton transfer between the two adjacent carbons of M6P and F6P.

The question about the binding mode (cyclic or linear) of the substrates M6P and F6P to PMI underlies the question of whether or not PMI catalyses the opening step of the substrates, mostly cyclic in solution. However, nothing is reported in the literature about this point. Answer to this question would probably constitute an entire study by itself, by using, as an example, cyclic substrate analogue inhibitors and/or substrates themselves. While we keep in mind this study, it is not the subject of this article which deals with transition state analogue inhibitors of the isomerization step of the linear substrates. The inhibitors used here, 5PAH and 5PAA, cannot form cyclic molecules.

The energy-minimized structures obtained in this study could, in the absence of actual crystal structures of PMI-inhibitor complexes, serve as starting points towards the design of novel inhibitors having increased affinities. Thus, energy computations should enable to quantify the contributions of the individual hydroxyl groups of 5PAH to the binding affinity, the effects of the chirality of the carbons bearing them, the effects of replacing one, or both, anionic moieties of 5PAH by other Zn(II)-ligating and electron-rich moieties, as well as those of extensions of the molecular structure. Such computations are now in progress, and should be useful into orienting chemical synthesis towards more effective inhibitors, enabling the model to evolve further on the basis of the experimental feedback.

As in our β-lactamase study, we provide as supporting information the pdb files of the nine 5PAH and 5PAA complexes with the PMI model. They are also posted on the Web site at http://www.lct/jussieu.fr/pagesperso/jpp.

Acknowledgments

The *ab initio* computations were performed on the computers of the Centre d'Informatique National de l'Enseignement Supérieur (CINES, Montpellier, France) of the Centre de Ressources Informatiques de Haute Normandie (CRIHAN, Rouen, France), and of the Institut de Developpement en Ressources Informatiques (IDRIS, Orsay, France). We wish to thank Nicole Audiffren (CINES) and Guy Moebs (CRIHAN) for their help. We wish to thank the two reviewers of this paper for constructive comments.

References

1. Slein, B. W. J Biol Chem 1950, 186, 753.
2. Gracy, R. W.; Noltmann, E. A. J Biol Chem 1968, 243, 3161.

3. Orlean, P. Mol Cell Biol 1990, 10, 5796.
4. Payton, M. A.; Rheinnecker, M.; Klig, L. S.; DeTiani, M.; Bowden, E. J Bacteriol 1991, 173, 2006.
5. Smith, D. J.; Proudfoot, A. E. I.; De Tiani, M.; Wells, T. N. C.; Payton, M. A. Yeast 1995, 11, 301.
6. Patterson, J. H.; Waller, R. F.; Jeevarajah, D.; Billman-Jacobe, H.; McConville, M. J. Biochem J 2003, 372, 77.
7. Garami, A.; Ilg, T. J Biol Chem 2001, 276, 6566.
8. Shinabarger, D.; Berry, A.; May, T. B.; Rothmel, R.; Fialho, A.; Chakrabarty, A. M. J Biol Chem 1991, 266, 2080.
9. Proudfoot, A. E. I.; Turcatti, G.; Wells, T. N. C.; Payton, M. A.; Smith, D. J. Eur J Biochem 1994, 219, 415.
10. Jensen, S. O.; Reeves, P. R. Biochem Biophys Acta 1998, 1382, 5.
11. Smith, D. J.; Payton, M. A. Mol Cell Biol 1994, 14, 6030.
12. Coulin, F.; Magnenat, E.; Proudfoot, A. E. I.; Payton, M. A.; Scully, P.; Wells, T. N. C. Biochemistry 1993, 32, 14139.
13. Cleasby, A.; Wonacott, A.; Skarzynski, T.; Hubbard, R. E.; Davies, G. J.; Proudfoot, A. E. I.; Bernard, A. R.; Payton, M. A.; Wells, T. N. C. Nat Struct Biol 1996, 3, 470.
14. Wells, T. N. C.; Scully, P.; Magnenat, E. Biochemistry 1994, 33, 5772.
15. Proudfoot, A. E. I.; Payton, M. A. J Protein Chem 1994, 13, 619.
16. Smith, J. J.; Thomson, A. J.; Proudfoot, A. E. I.; Wells, T. N. C. Eur J Biochem 1997, 244, 325.
17. Wills, E. A.; Roberts, I. S.; Del Poeta, M.; Rivera, J.; Casadevall, A.; Cox, G. M.; Perfect, J. R. Mol Microbiol 2001, 40, 610.
18. Miles, J. S.; Guest, J. R. Gene 1991, 32, 41.
19. Wells, T. N. C.; Payton, M. A.; Proudfoot, A. E. I. Biochemistry 1993, 32, 1294.
20. Wells, T. N. C.; Payton, M. A. Biochemistry 1994, 33, 7641.
21. Pitkänen, J.-P.; Törmä, A.; Alff, S.; Huopaniemi, S. P. M.; Renkonen, R. J Biol Chem 2004, 279, 55737.
22. Collins, L. V.; Hackett, J. Gene 1991, 103, 135.
23. Gracy, R. W.; Noltmann, E. A. J Biol Chem 1968, 243, 4109.
24. Griffin, A. M.; Poelwijk, E. S.; Morris, V. J.; Gasson, M. J. FEMS Microbiol Lett 1997, 154, 389.
25. Wu, B.; Zhang, Y.; Zheng, R.; Guo, C.; Wang, P. G. FEBS Lett 2002, 519, 87.
26. Ideguchi, T.; Hu, C.; Kim, B. H.; Nishise, H.; Yamashita, J.; Kakuno, T. Biochim Biophys Acta 1993, 1172, 329.
27. Jiang, X. M.; Neal, B.; Santiago, F.; Lee, S. J.; Romana, L. K.; Reeves, P. R. Mol Microbiol 1991, 5, 695.
28. Papoutsopoulou, S. V.; Kyriakidis, D. A. Mol Cell Biochem 1997, 177, 183.
29. Schmidt, M.; Arnold, W.; Niemann, A.; Kleickmann, A.; Puhler, A. Gene 1992, 122, 35.
30. Hansen, T.; Wendorff, D.; Schönheit, P. J Biol Chem 2004, 279, 2262.
31. Hansen, T.; Urbanke, C.; Schönheit, P. Extremophiles 2004, 8, 507.
32. Rose, I. A.; O'Connell, E. L. J Biol Chem 1961, 236, 3086.
33. Swan, M. K.; Solomons, J. T. G.; Beeson, C. C.; Hansen, T.; Schönheit, P.; Davies, C. J Biol Chem 2003, 278, 47261.
34. Berrisford, J. M.; Akerboom, J.; Brouns, S.; Sedelnikova, S. E.; Turnbull, A. P.; van der Oost, J.; Salmon, L.; Hardré, R.; Murray, I. A.; Blackburn, G. M. J Mol Biol 2004, 343, 649.
35. Seeholzer, S. H. Proc Natl Acad Sci USA 1993, 90, 1237.
36. Swan, M. K.; Hansen, T.; Schönheit, P.; Davies, C. J Biol Chem 2004, 279, 39838.
37. Swan, M. K.; Hansen, T.; Schönheit, P.; Davies, C. Biochemistry 2004, 43, 14088.
38. Jeffery, C. J.; Hardré, R.; Salmon, L. Biochemistry 2001, 40, 1560.
39. Lee, J. H.; Chang, K. Z.; Patel, V.; Jeffery, C. J. Biochemistry 2001, 40, 7799.
40. Arsenieva, D.; Jeffery, C. J. J Mol Biol 2002, 323, 77.
41. Arsenieva, D.; Hardré, R.; Salmon, L.; Jeffery, C. J. Proc Natl Acad Sci USA 2002, 99, 5872.
42. Davies, C.; Muirhead, H. Proteins 2002, 50, 577.
43. Solomons, J. T. G.; Zimmerly, E. M.; Burns, S.; Krishnamurthy, N.; Swan, M. K.; Krings, S.; Muirhead, H.; Chirgwin, J.; Davies, C. J Mol Biol 2004, 342, 847.
44. Malaisse-Lagae, F.; Liemans, V.; Yaylali, B.; Sener, A.; Malaisse, W. J. Biochim Biophys Acta 1989, 998, 118.
45. Roux, C.; Lee, J. H.; Jeffery, C. J.; Salmon, L. Biochemistry 2004, 43, 2926.
46. Gracy, R. W.; Noltmann, E. A. J Biol Chem 1968, 243, 5410.
47. DeLano, W. L. The PyMOL Molecular Graphics System; DeLano Scientific: San Carlos, CA, 2002.
48. Gresh, N. J Comput Chem 1995, 16, 856.
49. Gresh, N.; Roques, B.-P. Biopolymers 1997, 41, 145.
50. Garmer, D. R.; Gresh, N.; Roques, B.-P. Proteins 1998, 31, 42.
51. Antony, J.; Gresh, N.; Olsen, L.; Hemmingsen, L.; Schofield, C.; Bauer, R. J Comput Chem 2002, 23, 1281.
52. Antony, J.; Piquemal, J.-P.; Gresh, N. J Comput Chem 2005, 26, 1131.
53. Gresh, N.; Shi, G.-B. J Comput Chem 2004, 25, 160.
54. Gresh, N.; Sponer, J. J Phys Chem B 1999, 103, 11415.
55. Gresh, N.; Sponer, J. E.; Spacková, N.; Leszczynski, J.; Sponer, J. J Phys Chem B 2003, 107, 8669.
56. Gresh, N.; Derreumaux, P. J Phys Chem B 2003, 107, 4862.
57. Piquemal, J.-P.; Gresh, N.; Giessner-Prettre, C. J Phys Chem A 2003, 107, 10353.
58. Gresh, N.; Piquemal, J.-P.; Krauss, M. J Comput Chem 2005, 26, 1113.
59. Langlet, J.; Claverie, P.; Caillet, J.; Pullman, A. J Phys Chem 1988, 92, 1617.
60. Langlet, J.; Gresh, N.; Giessner-Prettre, C. Biopolymers 1995, 36, 765.
61. Garmer, D. R.; Stevens, W. J. J Phys Chem A 1989, 93, 8263.
62. (a) Huron, M. J.; Claverie, P. J Phys Chem 1972, 76, 2123; (b) Huron, M. J.; Claverie, P. J Phys Chem 1974, 78 1853.
63. Pierrotti, R. A. J Phys Chem 1965, 69, 2813.
64. Tannor, D. J.; Marten, B.; Murphy, R.; Friesner, R. A.; Sitkoff, D.; Nicholls, A.; Ringnalda, M.; Goddard, W. A., III; Honig, B. J Am Chem Soc 1994, 116, 11875.
65. Tomasi, J.; Persico, M. Chem Rev 1994, 94, 2027.
66. Ledecq, L.; Lebon, F.; Durant, F.; Giessner-Prettre, C.; Marquez, A.; Gresh, N. J Phys Chem B 2003, 107, 10640.
67. Gresh, N.; Kafafi, S. A.; Truchon, J.-F.; Salahub, D. R. J Comput Chem 2004, 25, 823.
68. Rogalewicz, F.; Gresh, N.; Ohanessian, G. J Comput Chem 2000, 21, 963.
69. Tiraboschi, G.; Fournie-Zaluski, M. C.; Roques, B. P.; Gresh, N. J Comput Chem 2001, 22, 1038.
70. Gresh, N.; Claverie, P.; Pullman, A. Theor Chim Acta 1984, 66, 1.
71. Evangelakis, G. A.; Rizos, J. P.; Lagaris, I. E.; Demetropoulos, I. N. Comput Phys Commun 1987, 46, 401.
72. Stevens, W. J.; Basch, H.; Krauss, M. J Chem Phys 1984, 81, 6026.
73. Hay, P. J.; Wadt, W. R. J Chem Phys 1985, 82, 299.
74. Lee, C.; Yang, W.; Parr, R. G. Phys Rev B 1988, 37, 785.
75. Becke, A. D. J Chem Phys 1993, 98, 5648.
76. Frisch, M. J.; Trucks, G. W.; Schlegel, H. B.; Scuseria, G. E.; Robb, M. A.; Cheeseman, J. R.; Montgomery, J. J. A.; Vreven, T.; Kudin, K. N.; Burant, J. C.; Millam, J. M.; Iyengar, S. S.; Tomasi, J.; Barone, V.; Mennucci, B.; Cossi, M.; Scalmani, G.; Rega, N.; Petersson, G. A.; Nakatsuji, H.; Hada, M.; Ehara, M.; Toyota, K.;

Fukuda, R.; Hasegawa, J.; Ishida, M.; Nakajima, T.; Honda, Y.; Kitao, O.; Nakai, H.; Klene, M.; Li, X.; Knox, J. E.; Hratchian, H. P.; Cross, J. B.; Bakken, V.; Adamo, C.; Jaramillo, J.; Gomperts, R.; Stratmann, R. E.; Yazyev, O.; Austin, A. J.; Cammi, R.; Pomelli, C.; Ochterski, J. W.; Ayala, P. Y.; Morokuma, K.; Voth, G. A.; Salvador, P.; Dannenberg, J. J.; Zakrzewski, V. G.; Dapprich, S.; Daniels, A. D.; Strain, M. C.; Farkas, O.; Malick, D. K.; Rabuck, A. D.; Raghavachari, K.; Foresman, J. B.; Ortiz, J. V.; Cui, Q.; Baboul, A. G.; Clifford, S.; Cioslowski, J.; Stefanov, B. B.; Liu, G.; Liashenko, A.; Piskorz, P.; Komaromi, I.; Martin, R. L.; Fox, D. J.; Keith, T.; Al-Laham, M. A.; Peng, C. Y.; Nanayakkara, A.; Challacombe, M.; Gill, P. M. W.; Johnson, B.; Chen, W.; Wong, M. W.; Gonzalez, C.; Pople, J. A. Gaussian 03, Revision B. 05; Gaussian Inc., Wallingford, CT, 2004.

77. Jaguar 6.0. Schrodinger Inc.: Portland, OR, 2005.
78. Murphy, R. B.; Beachy, M. D.; Friesner, R. A.; Ringnalda, M. N. J Chem Phys 1995, 103, 1481.
79. Duan, Y.; Wu, C.; Chowdhury, S.; Lee, M. C.; Xiong, G.; Zhang, W.; Yang, R.; Cieplak, P.; Luo, R.; Lee, T. J Comput Chem 2003, 24, 1999.
80. Case, D. A.; Cheatham II, T. E.; Darden, T.; Gohlke, H.; Luo, R.; Merz, Jr, K. M.; Onufriev, A.; Simmerling, C.; Wang, B.; Woods, R. J Comput Chem 2005, 26, 1668.
81. Luo, R.; David, L.; Gilson, M. K. J Comput Chem 2002, 23, 1244.
82. Tiraboschi, G.; Gresh, N.; Giessner-Prettre, C.; Pedersen, L. G.; Deerfield, D. W. J Comput Chem 2000, 21, 1011.
83. Tiraboschi, G.; Roques, B. P.; Gresh, N. J Comput Chem 1999, 20, 1379.
84. Gresh, N.; Leboeuf, M.; Salahub, D. R. In Modeling the Hydrogen Bond;Smith, G. A., Ed; Oxford University Press: Oxford, 1994. ACS Symposium Series, Vol. 569, p. 81.
85. Guo, H.; Gresh, N.; Roques, B. P.; Salahub, D. R. J Phys Chem B 2000, 104, 9746.